Table 5
Infiltrating cells, neutrophils, and cytokines in air pouches

	Wild-type mice ($n = 5$)		IL-18-deficient mice ($n = 5$)	
	MSU (−)	MSU (+)	MSU (−)	MSU (+)
Infiltrating cells ($\times 10^6$)	0.19 ± 0.08	1.41 ± 0.42**	0.20 ± 0.18	1.66 ± 0.41**
Neutrophils ($\times 10^6$)	0.12 ± 0.05	1.28 ± 0.40**	0.14 ± 0.12	1.46 ± 0.32**
IL-18 (pg/ml)	ND	ND	ND	ND
IL-1β (pg/ml)	<16.0	947.0 ± 595.4*	16.0	898.8 ± 679.7*
KC (pg/ml)	17.2 ± 8.6	652.9 ± 323.6*	18.2 ± 11.1	845.8 ± 318.9**
MIP-1α (pg/ml)	1.92 ± 0.52	52.8 ± 17.7**	2.50 ± 1.10	47.7 ± 26.9*
IL-6 (pg/ml)	<16	553.8 ± 306.6*	<16.0	748.6 ± 462.9*

Values are expressed as the mean ± SD. ND, not detected (<5 pg/ml). MSU (−) and MSU (+) denote without and with, respectively, the injection of MSU into air pouches. Significant differences between the variables were analyzed using ANOVA. *$P < 0.05$ and **$P < 0.01$, as compared with the respective value without the injection of MSU crystals. All parameters are not significantly different between wild-type mice with MSU (+) and IL-18-deficient mice with MSU (+).

containing MSU crystals were markedly increased as compared with those after the injection of PBS alone.

4. Discussion

IL-18 is a member of the interleukin-1 cytokine superfamily and is recognized as an important regulator of both innate and acquired immunity. It is produced in an inactive 24 kDa precursor form, which is cleaved by IL-1β converting enzyme (caspase 1) and proteinase 3 to generate a biologically active 18 kDa mature form. The active form of IL-18 is secreted by monocytes–macrophages, dendritic cells, and Kupffer cells, as well as some osteoblasts and keratinocytes [11–14]. Further, its mRNA expression is induced in the adrenal cortex [15] and the pancreas of nonobese diabetic mice [16]. Therefore, in addition to its role in the immune system, it has been suggested that IL-18 may play a role in connecting the immune system to other biological systems, such as the endocrine and nervous systems.

The definitive role of IL-18 is to produce interferon-γ, especially in the presence of IL-12, which accelerates inflammation. In addition, the cytokine augments NK cell activity and the cytotoxicity of TH1 cells [3,17,18] and itself has capabilities to induce IL-4, IL-5, IL-10, and IL-13 from T and NK cells [17,18]. Thus, the pro-inflammatory IL-18 plays a crucial role in the development and sustenance of inflammation, and may also have a relationship to the compensatory anti-inflammatory response [18]. Recent studies have demonstrated that serum levels of IL-18 are elevated in patients with rheumatoid arthritis [19,20], and that lipopolysaccharide (LPS) and purified protein derivative (PPD) stimulate monocytes to secrete IL-18 [21,22]. In addition, it has been shown that IL-18 promotes neutrophil accumulation [4]. Those results led us to speculate that MSU crystals stimulate synovial membranes and monocyte-macrophages to secrete IL-18 in the joints, and IL-18 plays some role, especially neutrophil accumulation, in gouty arthritis along with other cytokines. To test our hypothesis, we measured IL-18 levels together with TNF-α, IL-1β, IL-8, and IL-6 in gout patients in the presence of gouty arthritis.

In the present patients, the plasma concentration of IL-18 was elevated in the presence of gouty arthritis, as indicated by plasma CRP levels, when compared with in its absence. Further, in all patients with gouty arthritis, the plasma concentration of IL-18 was greater than 200 pg/ml (reference value below 200 pg/ml). Therefore, we also conducted an in vitro examination, which demonstrated that MSU crystals stimulate $CD14^-$ cells to secrete IL-18 (Fig. 1). These results suggest that the post-transcriptional regulation of IL-18 by MSU crystals may play a role in inflammation, since the presence of MSU crystals did not significantly affect IL-18 mRNA in $CD14^+$ cells (Fig. 2). Accordingly, we investigated effects of MSU crystals on caspase 1 and found that their presence increased caspase 1 activity in $CD14^+$ cells, while the caspase inhibitor Z-Val-Ala-Asp (Ome)-CH_2F significantly inhibited the secretion of IL-18 and IL-1β from MSU crystal-activated $CD14^+$ cells. In addition, in caspase 1-deficient mice, MSU crystals only slightly induced the secretion of IL-18 from TM-induced peritoneal cells (peritoneal macrophages). These results suggest that the MSU crystal-induced secretion of the active form of IL-18 from monocytes is mainly ascribed to the cleavage of the inactive form probably in an endogenous pool by caspase 1[23], though we did not measure the levels of the inactive form. As a result, IL-18 may be actively processed to mature protein in monocytes-macrophages by caspase-1 that has been activated by MSU crystals. However, the concentrations of IL-18 after the injection of PBS containing MSU crystals were below the limit of detection in pouch fluid from wild-type mice, suggesting that monocytes-macrophages in the air pouch pseudosynovial membranes may not play a significant role in the MSU crystal-induced secretion of IL-18.

A previous study demonstrated that IL-18 protein was produced by IL-1-stimulated chondrocytes obtained from healthy organ donors, suggesting that chondrocytes are potential source of IL-18 in the joints [24]. In addition, synovial tissue cells from the subjects with rheumatoid arthritis were found to express IL-18 mRNA and spontaneously produce IL-18 protein in vitro [25]. Another study demonstrated that CRP induced the secretion of IL-18 from human umbilical vein endothelial cells [26], suggesting that circulating CRP that is increased by gouty arthritis may stimulate the secretion of IL-18 from endothelial cells, though the present study did not show the relationship between CRP and IL-18 levels in gouty arthritis. Therefore, in patients with gouty arthritis, chondrocytes and synovial cells and/or CRP-stimulated endothelial cells may be sources of plasma IL-18.

In addition to its role of IL-18 inducing interferon-γ from activated Th 1 cells and NK cells, IL-18 also promotes neutrophil accumulation [4], which is intriguing for the study of gout. However, in the present IL-18-deficient mouse experiment, the cytokine did not play a significant role in MSU crystal-induced neutrophil accumulation. In contrast, the production of KC and MIP-1α was increased along with neutrophil accumulation in air pouches containing MSU crystals. Since it is known that KC plays a role in neutrophil accumulation in inflammation [27] and MIP-1α has been shown to be involved in neutrophil accumulation in specific experimental models [27], KC and MIP-1α seem to play a role in MSU-induced neutrophil accumulation. However, the full role of IL-18 in gouty arthritis could not be elucidated from the results of the present study and further examinations are needed.

Another purpose of the present study was to determine whether plasma concentrations of TNF-α, IL-1, IL-6, and IL-8 reflect a state of gouty arthritis. In gouty arthritis induced by MSU crystals, synoviocytes, monocyte-macrophages, platelets, and neutrophils are activated [2] and secrete many kinds of cytokines, including TNF-α, IL-1β, IL-6, and IL-8, that accelerate acute inflammation. In fact, substantial levels of these cytokines are found in synovial fluids from gouty arthritis patients, though it has not been reported whether the plasma concentrations of TNF-α, IL-1β, IL-6, IL-8, and CRP are elevated during the period of gouty arthritis. In the present gout patients, we found increases in the levels of plasma IL-6 and IL-8. Our results suggest that plasma levels of IL-18, IL-6, and IL-8 reflect local inflammation, such as that associated with gouty arthritis. In contrast, the plasma levels of TNF-α and IL-1β may not reflect that condition, though MSU crystals induce their release from monocytes-macrophages and synovial lining cells into the synovial fluid. Although it remains undetermined, these cytokines may remain localized in inflamed lesions or rapidly cleared from blood.

References

[1] Guerne PA, Terkeltaub R, Zuraw B, Lotz M. Inflammatory microcrystals stimulate interleukin-6 production and secretion by human monocytes and synoviocytes. Arthritis Rheum 1989;32:1443–52.

[2] Di Giovine FS, Malawista SE, Nuki G, Duff GW. Interleukin 1 (IL 1) as a mediator of crystal arthritis. Stimulation of T cell and synovial fibroblast mitogenesis by urate crystal-induced IL 1. J Immunol 1987;138:3213–8.

[3] Okamura H, Tsutsi H, Komatsu T, Yutsudo M, Hakura A, Tanimoto T, et al. Cloning of a new cytokine that induces IFN-gamma production by T cells. Nature 1995;378:88–91.

[4] Leung BP, Culshaw S, Gracie JA, Hunter D, Canetti CA, Campbell C, et al. A role for IL-18 in neutrophil activation. J Immunol 2001;167(5):2879–86.

[5] Wallace SL, Robinson H, Masi AT, Decker JL, McCarty DJ, Yu TF. Preliminary criteria for the classification of the acute arthritis of primary gout. Arthritis Rheum 1977;20:895–900.

[6] Roberge CJ, Gaudry M, de Medicis R, Lussier A, Poubelle PE, Naccache PH. Crystal-induced neutrophil activation. IV. Specific inhibition of tyrosine phosphorylation by colchicine. J Clin Invest 1993;92(4):1722–9.

[7] Kotake S, Schumacher Jr HR, Wilder RL. A simple nested RT-PCR method for quantitation of the relative amounts of multiple cytokine mRNAs in small tissue samples. J Immunol Methods 1996;199:193–203.

[8] Tsutsui H, Kayagaki N, Kuida K, Nakano H, Hayashi N, Takeda K, et al. Caspase-1-independent, Fas/Fas ligand-mediated IL-18 secretion from macrophages causes acute liver injury in mice. Immunity 1999;11(3):359–67.

[9] Takeda K, Tsutsui H, Yoshimoto T, Adachi O, Yoshida N, Kishimoto T, et al. Defective NK cell activity and Th1 response in IL-18-deficient mice. Immunity 1998;8(3):383–90.

[10] Terkeltaub R, Baird S, Sears P, Santiago R, Boisvert W. The murine homolog of the interleukin-8 receptor CXCR-2 is essential for the occurrence of neutrophilic inflammation in the air pouch model of acute urate crystal-induced gouty synovitis. Arthritis Rheum 1998;41(5):900–9.

[11] Tsutsui H, Matsui K, Okamura H, Nakanishi K. Pathophysiological roles of interleukin-18 in inflammatory liver diseases. Immunol Rev 2000;174:192–209.

[12] Yu Y, Hagihara M, Ando K, Gansuvd B, Matsuzawa H, Tsuchiya T, et al. Enhancement of human cord blood CD34 cell-derived NK cell cytotoxicity by dendritic cells. J Immunol 2001;166:1590–600.

[13] Udagawa N, Horwood NJ, Elliott J, Mackay A, Owens J, Okamura H, et al. Interleukin-18 (interferon-gamma-inducing factor) is produced by osteoblasts and acts via granulocyte/macrophage colony-stimulating factor and not via interferon-gamma to inhibit osteoclast formation. J Exp Med 1997;185:1005–12.

[14] Stoll S, Muller G, Kurimoto M, Saloga J, Tanimoto T, Yamauchi H, et al. Production of IL-18 (IFN-gamma-inducing factor) messenger RNA and functional protein by murine keratinocytes. J Immunol 1997;159:298–302.

[15] Sugama S, Kim Y, Baker H, Tinti C, Kim H, Joh TH, et al. Tissue-specific expression of rat IL-18 gene and response to adrenocorticotropic hormone treatment. J Immunol 2000;165:6287–92.

[16] Rothe H, Hausmann A, Casteels K, Okamura H, Kurimoto M, Burkart V, et al. IL-18 inhibits diabetes development in nonobese diabetic mice by counterregulation of Th1-dependent destructive insulitis. J Immunol 1999;163:1230–6.

[17] Vervoordeldonk MJ, Tak PP. Cytokines in rheumatoid arthritis. Curr Rheumatol Rep 2002;4(3):208–17.

[18] Kashiwamura S, Ueda H, Okamura H. Roles of interleukin-18 in tissue destruction and compensatory reactions. J Immunother 2002;25(Suppl. 1):S4–11.

[19] Yamamura M, Kawashima M, Taniai M, Yamauchi H, Tanimoto T, Kurimoto M, et al. Interferon-gamma-inducing activity of interleukin-18 in the joint with rheumatoid arthritis. Arthritis Rheum 2001;44:275–85.

[20] Kawashima M, Yamamura M, Taniai M, Yamauchi H, Tanimoto T, Kurimoto M, et al. Levels of interleukin-18 and its binding inhibitors in the blood circulation of patients with adult-onset Still's disease. Arthritis Rheum 2001;44:550–60.

[21] Seki E, Tsutsui H, Nakano H, Tsuji N, Hoshino K, Adachi O, et al. Lipopolysaccharide-induced IL-18 secretion from murine Kupffer cells independently of myeloid differentiation factor 88 that is critically involved in induction of production of IL-12 and IL-1beta. J Immunol 2001;166:2651–7.

[22] Vankayalapati R, Wizel B, Weis SE, Samten B, Girard WM, Barnes PF. Production of interleukin-18 in human tuberculosis. J Infect Dis 2000;182:234–9.

[23] Gu Y, Kuida K, Tsutsui H, Ku G, Hsiao K, Fleming MA, et al. Activation of interferon-gamma inducing factor mediated by interleukin-1beta converting enzyme. Science 1997;275:206–9.

[24] Olee T, Hashimoto S, Quach J, Lotz M. IL-18 is produced by articular chondrocytes and induces proinflammatory and catabolic responses. J Immunol 1999;162:1096–100.

[25] Yamamura M, Kawashima M, Morita Y, Makino H, Tanimoto T, Kurimoto M. Increased production of interleukin-18 in synovium from patients with rheumatoid arthritis. Arthritis Rheum 1997;40:s274.

[26] Yamaoka-Tojo M, Tojo T, Masuda T, Machida Y, Kitano Y, Kurosawa T, et al. C-reactive protein-induced production of interleukin-18 in human endothelial cells: a mechanism of orchestrating cytokine cascade in acute coronary syndrome. Heart Vessels 2003;18(4):183–7.

[27] Garcia-Ramallo E, Marques T, Prats N, Beleta J, Kunkel SL, Godessart N. Resident cell chemokine expression serves as the major mechanism for leukocyte recruitment during local inflammation. J Immunol 2002;169(11):6467–73.

doi:10.1093/intimm/dxl005

The ubiquitin–proteasome system plays essential roles in presenting an 8-mer CTL epitope expressed in APC to corresponding CD8$^+$ T cells

Xuefeng Duan[1], Hajime Hisaeda[1], Jianying Shen[1], Liping Tu[1], Takashi Imai[1], Bin Chou[1], Shigeo Murata[2], Tomoki Chiba[2], Keiji Tanaka[2], Hans Jörg Fehling[3], Takaomi Koga[4], Katsuo Sueishi[4] and **Kunisuke Himeno[1]**

[1]Department of Microbiology and Immunology, Graduate School of Medical Sciences, Kyushu University, Fukuoka, Japan
[2]Department of Molecular Oncology, Tokyo Metropolitan Institute of Medical Science, Tokyo, Japan
[3]Department of Immunology, University of Ulm, Ulm, Germany
[4]Department of Pathology, Graduate School of Medical Sciences, Kyushu University, Fukuoka

Keywords: antigen presentation, ubiquitin-fusion degradation pathway

Abstract

MUT1 is an H-2K^b-restricted 8-mer CTL epitope expressed in Lewis lung carcinoma (3LL) tumor cells derived from C57BL/6 (B6) mice. We constructed a chimeric gene encoding ubiquitin-fused MUT1 (pUB-MUT1). By using a gene gun, B6 mice were immunized with the gene prior to challenge with 3LL tumor cells. Tumor growth and lung metastasis were prominently suppressed in mice immunized with pUB-MUT1 but only slightly in those immunized with the MUT1 gene (pMUT) alone. CD8$^+$ T cells were confirmed to be the final effector by *in vitro* experiments and *in vivo* removal of the cells with a corresponding antibody. Anti-tumor immunity was profoundly suppressed in mice deficient in an immuno-subunit of proteasome, LMP7. Furthermore, mice deficient in a proteasome regulator, PA28α/β, failed to acquire protective immunity. Thus, application of the ubiquitin-fusion degradation pathway was useful even in immunization with genes encoding a single CTL epitope for induction of specific and active CD8$^+$ T cells.

Introduction

Since the 1980s, several tumor-associated antigens (TAAs) and CD8$^+$ T cell epitopes in those antigens have been identified and cloned (1–4). However, it has been hard to induce active CD8$^+$ CTL responses by conventional peptide/epitope-based vaccines (5). Host immunity, including CTL response to TAAs, is hyporesponsive or has developed immunological tolerance since most TAAs are poorly immunogenic self-antigens (6, 7). Although CTL responses are readily generated by live/live-attenuated vaccines (8–10), such vaccines have several problems that preclude their widespread use. Recently, vaccines using genes encoding TAAs have been developed by many investigators, and these have been expected to mimic the effect of live-attenuated vaccines in their ability to induce MHC class I-restricted CD8$^+$ T-cell responses (11–23). In such DNA vaccination, co-delivery of TAA genes with those that encode cytokines such as granulocyte macrophage colony-stimulating factor and IL-12 is usually required. However, these cytokines inevitably have side effects.

Antigen presentation to CD8$^+$ T cells is mediated by MHC class I molecules expressed on antigen-presenting cells (APCs)/dendritic cells. Primarily, CD8$^+$ T cells recognize MHC class I-associated peptides derived from endogenous antigens, such as oncogene products or viral antigens, located in the cytosol. Prior to antigen presentation by MHC class I molecules, cytosolic antigens must be polyubiquitinated and processed to CTL epitopes by the proteasome. This pathway is termed the ubiquitin–proteasome system (UPS) (24–26). Early studies have indicated that this pathway is divided into two steps: substrate recognition, brought about by the ubiquitin conjugation system, and degradation, catalyzed by the 26S proteasome. During the recognition step, the ubiquitin-activating enzyme E1 activates ubiquitin in an ATP-requiring reaction to generate a high-energy thiol ester intermediate. One of several E2 proteins (ubiquitin-carrier proteins or ubiquitin-conjugating enzymes) transfers the activated ubiquitin moiety from E1, via an additional high-energy

Correspondence to: K. Himeno; E-mail: himeno@parasite.med.kyushu-u.ac.jp
Revised 21 October 2005, *accepted* 31 January 2006
Transmitting editor: T. Sasazuki
Advance Access publication 28 March 2006

thiol ester intermediate to the substrate that is specifically bound to a member of the ubiquitin–protein ligase family, E3. E3s catalyze the last step in the conjugation process; covalent attachment of ubiquitin to the substrate. The ubiquitin molecule is generally transferred to an ε-NH_2 group of an internal lysine residue in the substrate to generate a covalent isopeptide bond between the C-terminal Gly^{76} of ubiquitin and the ε-NH_2 group. Ubiquitin itself is often a substrate for further ubiquitination, and proteins modified by such multiubiquitin chains are preferentially targeted for degradation by the proteasome (27, 28).

One fascinating strategy for enhancing CTL responses to low antigenic peptides may be to increase the efficiency of antigen processing by, for example, using a gene that encodes a ubiquitin-fused version of the target peptide. Previous work has shown that artificially fused proteins bearing a non-removable N-terminal ubiquitin moiety, replacing the C-terminal Gly^{76} of ubiquitin with Ala or Val (29, 30), are readily degraded by UPS. The proteolytic system involved is termed the ubiquitin-fusion degradation pathway (UFD) (27, 31). In our previous experiment, we constructed a chimeric DNA encoding a fusion protein linking murine ubiquitin to the N-terminus of a full-length murine melanocyte antigen, tyrosinase-related protein 2 (TRP-2), to introduce into the UFD. C57BL/6 (B6) mice immunized with the DNA acquired potent anti-tumor immunity against B16 melanoma mediated by specific CTL (32). Vaccination activated $CD8^+$ T cells specific for autologous TRP-2, although conventional DNA vaccination with the gene encoding only TRP-2 failed to break the tolerance to self-TRP-2 and to develop anti-tumor immunity.

CTL epitopes in TAA peptides are 8–10 amino acids long and are presented to CTL by MHC class I molecules on the APC. There have been some reports on the use of edited epitope genes in DNA vaccines (33–37), but these vaccines have not always been successful in inducing active CTL and/or protective immunity. It is immunologically and clinically important to clarify whether vaccination with a gene encoding only a single CTL epitope in TAAs can induce potent CTL activity when the gene has been fused with a ubiquitin gene. In other words, it should be established whether DNA vaccines with genes for 8–10 amino acid peptides can effectively induce specific CTLs if they have been directed toward UFD, as was the case with a full-length peptide TRP-2, as described above.

The eight-amino acid-long TAA (4) MUT1 is a mutant with a substitution of a highly conserved Cys 54 to Gln 54 in the mouse gap junction protein connexin 37 (Con 37) expressed in vascular endothelial cells, and this mutant MUT1 gene has been confirmed to be a CTL epitope of TAAs expressed in Lewis lung carcinoma (3LL) derived from B6 mice (38). In the present study, we constructed a fusion gene encoding an 8-mer MUT1 and ubiquitin. B6 mice immunized with the fusion gene acquired potent anti-tumor immunity against 3LL tumor cells despite the fact that vaccination with the gene encoding only MUT1 was not effective. We demonstrated that UFD plays an essential role in inducing activated $CD8^+$ T cells even when a single CTL epitope is used as an immunogen, as was the case in the system with a full-length TRP-2 and melanoma. In the present study, mice deficient in proteasome-associated gene, LMP7 or PA28α/β, were used to confirm this conclusion.

Methods

Animals and tumors

Female B6 mice aged 7 weeks were purchased from Seac Yoshitomi (Fukuoka, Japan) and experiments were performed in accordance with the institutional guidelines of Kyushu University, Japan. Proteasome activator PA28 knockout ($PA28\alpha^{-/-}/\beta^{-/-}$) and immunoproteasome subunit LMP7 knockout ($LMP7^{-/-}$) mice of B6 background were established by our group (31, 39). 3LL, a highly metastatic and poorly immunogenic tumor cell line, was a generous gift from Cell Resource Center for Biomedical Research Institute of Development, Aging and Cancer, Tohoku University (Sendai, Japan) and was maintained in RPMI 1640 media supplemented with 10% fetal bovine serum, 100 IU ml^{-1} penicillin, 100 μg ml^{-1} streptomycin, 20 mM *N*-2-hydroxyethylpiperazine-*N'*-2-ethanesulfonic acid, 50 mM $NaHCO_3$ and 2 mM L-glutamine.

Plasmid construction

The plasmid pUB-MUT1 introducing the ubiquitin-fused MUT1 antigen was constructed by directly designing the MUT1 sequence into the anti-sense primer 5′-ATGGATCCCGGCTGGGCTGTGTTCTGCTCAAAGGCACCTCTCAGG-3′ and using the sense primer 5′-TCGAATTCGTTAACAGGTCAAAATGCAG-3′ to amplify the pUB vector (32) that we constructed. The gene was then inserted into *Eco*RI and *Bam*HI sites of pcDNA3.1(−). The gene encoding the MUT1 epitope without ubiquitination was amplified by PCR using sense 5′-TCGGTACCATGGTTTTTGAGCAGAACACAGCCCAGCCGGACTGTGCCTTC-3′ and anti-sense 5′-AGCTCCCGGGAGCTTTTTGCAAAA-3′ primers, using pcDNA3.1(−) as the template. The gene was then inserted into the *Kpn*I and XmaI sites of pcDNA3.1(−).

In vivo gene transfer and implantation of 3LL tumor cells

We used a Helios Gene Gun (BioRad, NY, USA) as described previously (32, 40–42). B6 mice were immunized three times with 6 μg plasmid at 1-week intervals using a control vector, pUB, pMUT1 or pUB-MUT1. Ten days after the final vaccination, 1×10^5 3LL tumor cells in 50 μl PBS were implanted into the left footpad of B6 mice, and tumor growth was evaluated by footpad swelling. The swelling size was calculated by subtracting the thickness of the right footpad from that of the left footpad after measuring with a caliper twice weekly. For the experiment on lung metastasis, B6 mice were intravenously challenged with 2×10^5 3LL tumor cells in 200 μl PBS. Twenty-eight days after challenge, mice were sacrificed and then all lobes of both lungs were dissected out and weighed.

Cytotoxicity assay

Mice were sacrificed at the time of tumor challenge and their spleen cells (4×10^7) were co-cultured with MUT1 peptide (4 μg ml^{-1}) in six-well culture plates in complete RPMI 1640 medium. After 3 days culture, graded numbers of viable effector cells were placed into round-bottomed 96-well plates with 1×10^4 [^{3}H]thymidine-labeled EL4 cells, which were pulsed with MUT1 peptide (4 μg ml^{-1}) for 2 h. After 6 h incubation, the cells were harvested onto glass-fiber filters and radioactivity was counted using a β scintillation counter, and specific killing was calculated as described previously (43).

Measurement of IFN-γ production

Ten days after the third immunization, mice were sacrificed and spleen cells were isolated. Twenty million splenocytes were co-cultured with or without MUT1 epitope for 48 h at 20 μg ml^{-1}. Then the supernatant was collected and IFN-γ production was measured by ELISA.

In vivo depletion of T cell subsets

Anti-CD4 mAb (clone GK1.5) or anti-CD8 mAb (clone 2.43) was injected intra-peritoneally at 0.5 mg per mouse on days −3 and −1 of tumor challenge. Tumor cells were inoculated on day 0. Depletion of each T cell subset was confirmed by flow cytometry; >95% of the appropriate cell subset was depleted.

In vitro transfection and western blotting

One hundred thousand COS-7 cells in a 2.5-cm-diameter dish (Nunc, Roskilde, Denmark) were transfected with 2 μg pMUT1 or pU-MUT1 by using Lipofectamine (Invitrogen, Carlsbad, CA, USA) with or without the proteasome inhibitor epoxomicin (Sigma, St Louis, MO, USA). Twenty-four hours after transfection, cell lysates were prepared by adding 200 μl lysis buffer (50 mM Tris–HCl, 1% Nonidet P-40/1% SDS, 1 μM leupeptin/100 μM phenylmethylsulfonylflouride, 1 μM pepstatin A and 100 μM EDTA), and 15 μg protein was used for western blotting with anti-ubiquitin (Medical & Biological Laboratories, Japan) as the first antibody. Peroxidase-conjugated anti-mouse IgG (H + L) (Zymed Laboratories, San Francisco, CA, USA) was used as the second antibody. Binding antibody was detected by using enhanced chemiluminescence reagents (Amersham Life Science, Buckinghamshire, UK).

Results

Anti-tumor immunity against 3LL tumor cells in mice immunized with pUB-MUT1 expression vectors

As a candidate gene for a DNA vaccine against murine 3LL tumor, we prepared an expression vector termed pMUT1 encoding the MUT1 epitope, which is a mutant with a substitution of a highly conserved Cys 54 to Gln 54 in mouse gap junction protein Con 37 (aa 52–59) in mouse 3LL tumor cells. We also constructed pUB-MUT1 encoding modified ubiquitin (G76A) at the N-terminus of the MUT1 epitope so as not to be cleaved by ubiquitin C-terminal hydrolases (Fig. 1), and we examined the effect of DNA vaccination on the 3LL *in vivo* and *in vitro*. In our study, B6 mice immunized with pMUT1 showed the same level of tumor growth as that in mice immunized with the control vector or pUB (Fig. 2A). In contrast, tumor growth in the mice immunized with pUB-MUT1 was much slower compared with that in the other three groups. More than 15% of pUB-MUT1-immunized mice remained tumor free until the end of the experiment (data not shown). Lung metastasis was almost completely suppressed in the pUB-MUT1-immunized group as evaluated by lung weight (Fig. 2B). Histological analysis also demonstrated that there was no sign of metastasis in these mice. In sharp contrast, multiple metastatic lesions were observed in mice in the other groups (Fig. 2C). Immunization of B6 mice with pUB-MUT1 did not affect growth of B16F1 melanoma cells, which are derived from B6 mice but do not express MUT1 antigen (Fig. 2D),

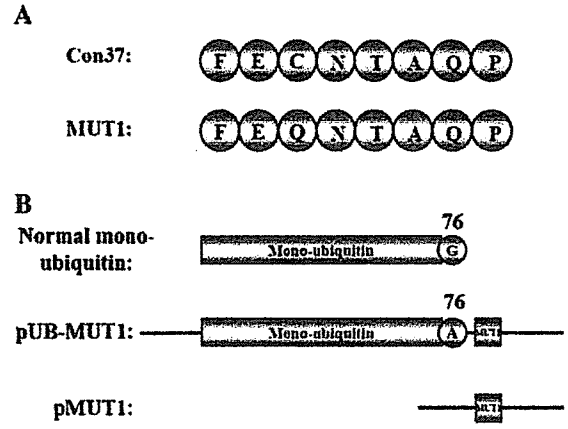

Fig. 1. (A) Amino acid sequences of Con 37 (aa 52–59) and MUT1. The eight-amino acid-long TAA peptide MUT1 is derived from mutation of a highly conserved Cys 54 to Gln 54 in the mouse gap junction protein Con 37 from the spontaneous C57BL/6 3LL. (B) Sketch map of normal mono-ubiquitin, pUB-MUT1 and pMUT1.

indicating that anti-tumor immunity induced by pUB-MUT1 immunization is highly antigen specific. Thus, immunization with pUB-MUT1, but not pMUT1, induces strong anti-tumor immunity *in vivo* against 3LL tumor cells.

Activation of $CD8^+$ T cells in mice immunized with pUB-MUT1

To determine the effector cells in the observed protective immunity, mice immunized with pUB-MUT1 were treated with anti-CD4 or anti-CD8 antibody to deplete the corresponding T cell subset, and then 3LL tumor cells were implanted. As shown in Fig. 3(A), anti-CD8 treatment completely abolished the anti-tumor immunity induced by pUB-MUT1 immunization. In contrast, treatment with control IgG or anti-CD4 antibody did not alternate the anti-tumor immunity, indicating that the immunity induced by pUB-MUT1 immunization is mediated by MUT1-specific $CD8^+$ T cells.

We next examined the function of $CD8^+$ T cells from mice immunized with MUT1-expressing plasmids by assessing CTL activity and IFN-γ production. We isolated splenocytes from various groups of B6 mice that had been immunized with pUB-MUT1, pMUT1, pUB or the control vector. Splenocytes from mice immunized with pUB-MUT1 vaccine showed prominent CTL activity against syngeneic EL4 target cells pulsed with MUT1 epitopes (Fig. 3B), and generated a remarkable amount of IFN-γ when cultured with 20 μg ml^{-1} MUT1 epitope compared with the other groups of mice (Fig. 3C).

Polyubiquitination and proteasomal processing of ubiquitin-fused MUT1 epitope

We previously reported that a full-length melanoma/melanocyte peptide, TRP-2, must be processed by UPS prior to the activation of TRP-2-specific $CD8^+$ T cells. In the present study, we employed the MUT1 gene, which encodes only a single 8-mer epitope for $CD8^+$ T cells, as a vaccine candidate. Immunization with pMUT1 scarcely induced activated $CD8^+$ T cells. On the other hand, immunization with pUB-MUT1 induced potent anti-tumor immunity mediated by $CD8^+$ T cells specific for the epitope, suggesting that processing via UPS is a critical step, even for a $CD8^+$ T cell-specific 8-mer epitope,

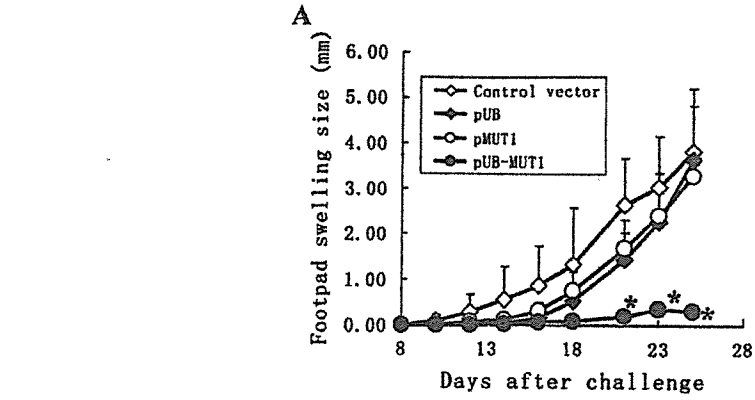
A
Footpad swelling size (mm)
6.00
5.00
4.00
3.00
2.00
1.00
0.00
Control vector
pUB
pMUT1
pUB-MUT1
8
13
18
23
28
Days after challenge

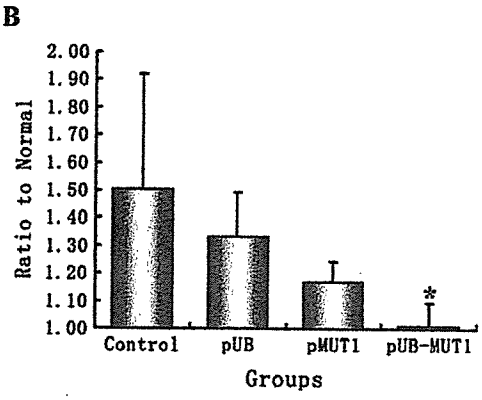
B
Ratio to Normal
2.00
1.90
1.80
1.70
1.60
1.50
1.40
1.30
1.20
1.10
1.00
Control
pUB
pMUT1
pUB-MUT1
Groups

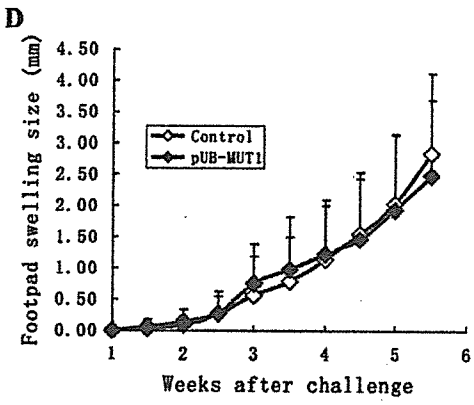
D
Footpad swelling size (mm)
4.50
4.00
3.50
3.00
2.50
2.00
1.50
1.00
0.50
0.00
Control
pUB-MUT1
1
2
3
4
5
6
Weeks after challenge

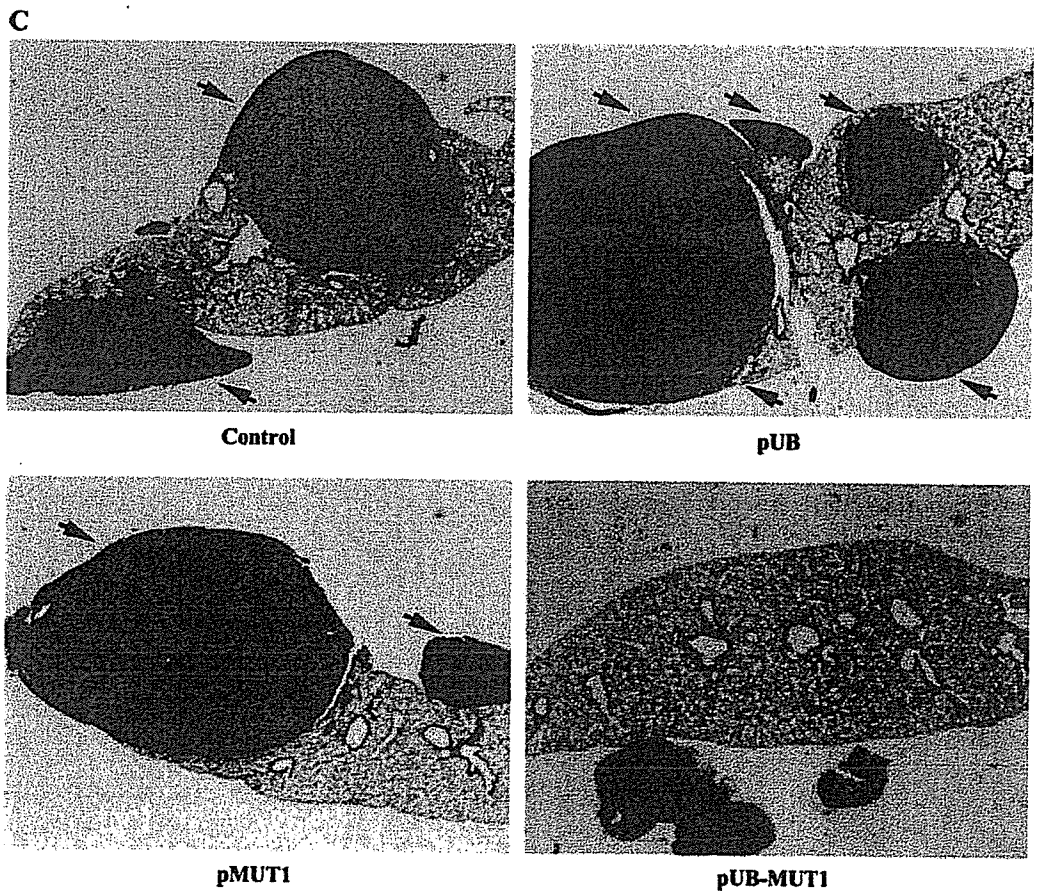
C
Control
pUB
pMUT1
pUB-MUT1

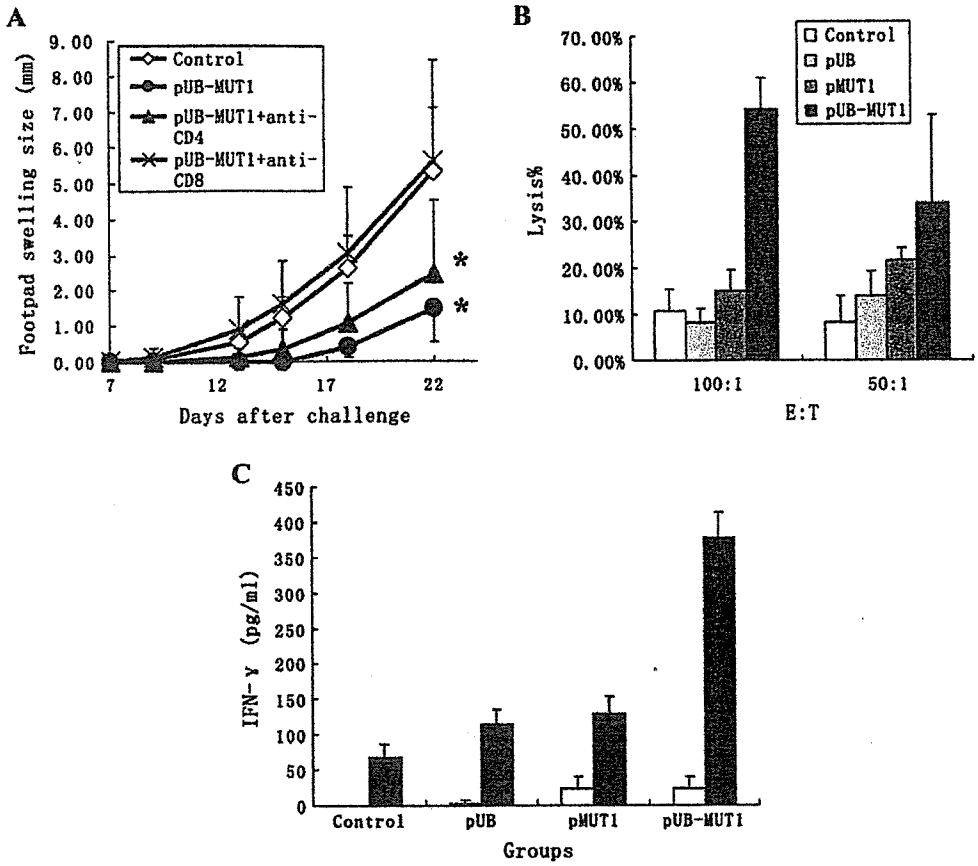

Fig. 3. Critical roles of $CD8^+$ T cells in anti-tumor immunity induced by pUB-MUT1. (A) Effect of depletion of $CD8^+$ T cells on anti-tumor immunity. Mice that had been immunized with pUB-MUT1 were treated with anti-CD4 or anti-CD8 antibody on days −3 and −1 of tumor challenge. Tumor growth was evaluated by footpad swelling. Each value is the average ± SD from six mice in each group. Complete depletion of the corresponding T cells was confirmed by flow cytometry (data not shown). Splenocytes isolated from mice 10 days after the final vaccination were analyzed for lytic activity (B) and production of IFN-γ (C). (B) Radio-labeled EL4 cells (1×10^4) pulsed with MUT1 were cultured with spleen cells at different effector-to-target ratios. CTL activity was not observed in the absence of MUT1 (data not shown). (C) Amounts of IFN-γ in supernatants from splenocytes cultured with (filled bars) or without (open bars) MUT1 epitope were determined by the ELISA method. Each value is the average ± SD from triplicate culture. Asterisks indicate statistically significant decreases compared with the control group.

prior to presentation on specific cells. To elucidate the difference between pMUT1 and pUB-MUT1 in the polyubiquitination and the processing via proteasomes, COS-7 cells transfected with pMUT1 or pUB-MUT1 were cultured in the presence or absence of proteasome inhibitor epoxomicin. Bands containing ubiquitin were not detected in cells transfected with pMUT1. One possibility is that polyubiquitination did not occur in these cells because MUT1 does not include lysine residues, acceptors of ubiquitination (28). COS-7 cells transfected with pUB-MUT1 contained not only a ubiquitin–MUT1 band but also additional upper bands consisting of polyubiquitinated products (Fig. 4A). Epoxomicin increased protein expression 1.5-fold (Fig. 4C). These results suggest that fusion of ubiquitin to the 8-mer MUT1 epitope made it susceptible to polyubiquitination, and processing by UPS.

Defective induction of anti-tumor immunity by immunization with pUB-MUT1 in LMP7$^{-/-}$ and PA28$\alpha^{-/-}/\beta^{-/-}$

In order to clarify whether ubiquitin-fused $CD8^+$ T cell epitope requires to go through the proteasome to efficiently activate precursor $CD8^+$ T cells, we used immunoproteasome subunit LMP7-deficient and proteasome regulator PA28α/β complex-deficient mice. After challenging with 3LL tumor cells, the same tendency was seen in LMP7 knockout mice, although it was not always in a completely dependent manner (Fig. 5).

Anti-tumor immunity was almost completely abolished in PA28-deficient mice compared with wild-type B6 mice

Fig. 2. Induction of antigen-specific anti-tumor immunity by vaccination with pUB-MUT1. B6 mice were immunized with the indicated plasmid, and 1×10^5 3LL tumor cells were implanted into the left footpad of each mouse. Tumor growth was evaluated by footpad swelling (A). Each value is the average ± SD from six mice in each group. Asterisks indicate statistical significance at $P < 0.02$ by the *t*-test. Vaccinated mice were intravenously challenged with 2×10^5 3LL tumor cells, and lung metastasis was analyzed by weighing lungs (B) and by histological examination (C). Asterisks indicate statistical significance at $P < 0.05$ by the *t*-test. Arrowheads indicate metastatic tumor lesions. (D) B6 mice that had been vaccinated with the indicated plasmid were challenged with 1×10^5 B16F1 melanoma cells, which do not express MUT1 antigen. Tumor growth was evaluated by footpad swelling. Each experiment was repeated at least three times and gave similar results.

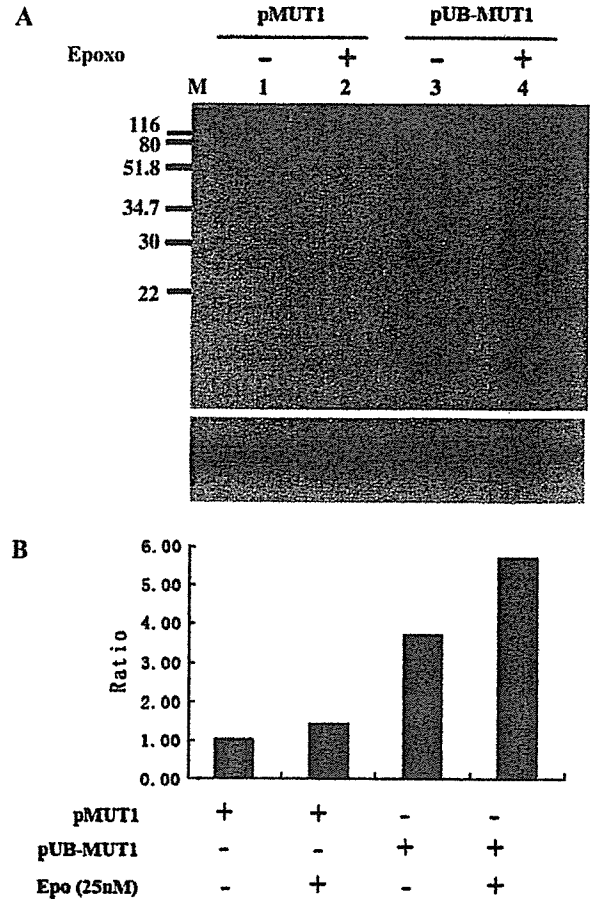

Fig. 4. Fusion of ubiquitin made the MUT1 epitope susceptible to polyubiquitination and processing by UPS. Plasmid-transfected COS-7 cells were cultured in the presence or absence of a proteasome inhibitor, epoxomicin. Twenty-four hours after transfection, cells were harvested and analyzed by western blotting using an anti-ubiquitin antibody (A, upper panel) or anti-HSP90 antibody as an internal control (A, lower panel). (B) Expression of MUT1 and UB-MUT1 were densitometrically quantified. Results represent the relative ratio of MUT1 level in COS-7 cells transfected with pMUT1 in the absence of epoxomicin after normalization with HSP90 expression.

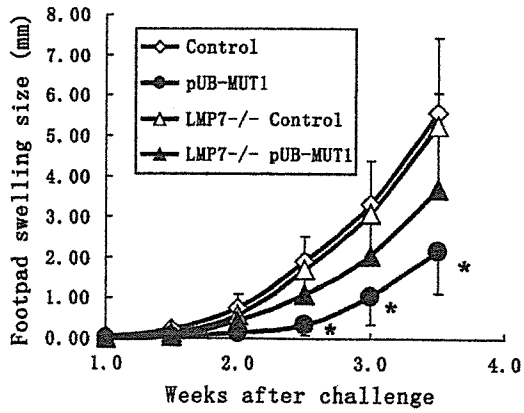

Fig. 5. Protective effect induced by the pUB-MUT1 was just partly cancelled in the LMP7$^{-/-}$ mice. B6 mice and LMP7$^{-/-}$ mice that had been vaccinated with pUB-MUT1 were challenged with 1×10^5 3LL tumor cells implanted into the left footpad. Asterisks indicate statistical significance at $P < 0.05$. This experiment was repeated at least three times and gave similar results.

(Fig. 6A). Furthermore, PA28-deficient mice completely failed to acquire anti-tumor immunity, as evaluated by either tumor growth inhibition or prevention of lung metastasis after immunization with pUB-MUT1 (Fig. 6B).

These results suggest, again, that even the 8-mer MUT1 epitope used in our study must be further handled by the UPS prior to presentation on MHC class I molecules and activating specific CD8$^+$ T cells, as in the case of the full-length TRP-2 (32).

Discussion

We previously developed a DNA vaccine with an expressing plasmid encoding a fusion protein between full-length TRP-2, a melanoma antigen, and ubiquitin. Immunization with the DNA vaccine resulted in remarkable activation of CD8$^+$ T cells specific for TRP-2 and induction of robust anti-melanoma immunity, presumably by preferential leading of ubiquitin-fused TRP-2 to the proteasomes and enhancement of its

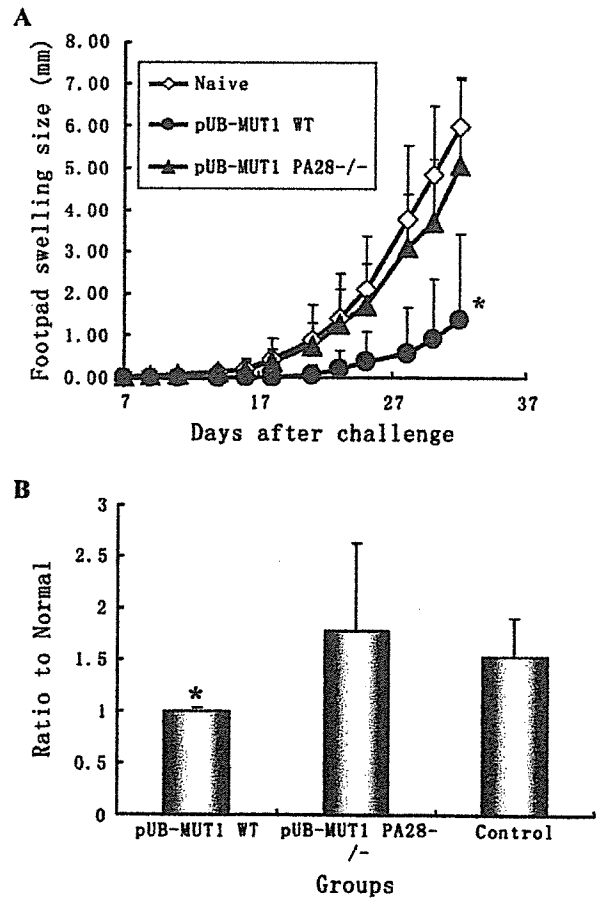

Fig. 6. Impaired pUB-MUT1 vaccination induced anti-tumor immunity in PA28$\alpha^{-/-}/\beta^{-/-}$ mice. (A) B6 mice and PA28$\alpha^{-/-}/\beta^{-/-}$ mice that had been vaccinated with pUB-MUT1 were challenged with 1×10^5 3LL tumor cells implanted into the left footpad. (B) Mice immunized with pUB-MUT1 were inoculated with 2×10^5 3LL tumor cells intravenously. Twenty-eight days after inoculation, mice were sacrificed and the lungs were weighed. Asterisks indicate statistical significance at $P < 0.05$ by the *t*-test. Each experiment was repeated at least three times and gave similar results.

degradation (32). Thus, ubiquitination of tumor antigens could be an ingenious strategy for inducing anti-tumor immunity.

In the present study, we exploited a DNA vaccine for a lung cancer, 3LL, by constructing a gene encoding MUT1, a CTL epitope with an 8-mer peptide but not a full-length protein. The pMUT1 encoding only MUT1 could not induce immunity against 3LL tumor cells, as evaluated by tumor growth, survival rate, and lung metastasis. Interestingly, vaccination with pUB-MUT1 encoding MUT1 fused with ubiquitin at the N-terminus efficiently induced MUT1-specific $CD8^+$ T cells (Fig. 3) and conferred mice with protective anti-tumor immunity (Fig. 2). Thus, the expression of MUT1 alone within cells appears not to be sufficient to induce $CD8^+$ CTLs specific for the epitope, whereas CTLs are potently activated when the CTL epitope has been ubiquitinated, and then processed via UPS and presented to MHC class I molecules. The difference in anti-tumor immunity between pMUT1 and pUB-MUT1 may be that the gene product in the latter is efficiently manipulated by UPS, and the process should be a crucial step of induction of CTL even when a gene encoding single 8-mer epitope is used as an immunogen. It should be noteworthy that $CD8^+$ T cells are also activated without support from $CD4^+$ helper T cells in our study, as some authors reported (32, 44–46).

Recently, a new ubiquitination factor, E4, has been found (47). E4 protein does not participate in the ubiquitin–enzyme thioester cascade. Moreover, in striking contrast to E3s, E4 does not interact with the substrate directly, but apparently with the ubiquitin moieties of ubiquitin–substrate conjugates. It is a crucial switch, which triggers degradation by adding just one or two ubiquitin moieties to the conjugate and may be important for regulating degradation of proteins already primed for degradation by oligoubiquitination. In this escort pathway to the proteasome, UFD, a protein substrate is modified by one or two ubiquitin moieties using E1, E2 and E3 enzymes. Based on the recognition of the oligoubiquitinated substrate by $CDC48^{UFD1/NPL4}$, E4 extends the ubiquitin chain by a few extra ubiquitin moieties. Subsequently, the ubiquitin–protein conjugate is delivered to the proteasome for degradation by the binding of RAD23 or DSK2 (48). In our system, ubiquitin-fused MUT1 antigen may be easily recognized by $CDC48^{UFD1/NPL4}$ and therefore efficiently delivered to the proteasome.

The immunomodulatory cytokine IFN-γ, which is produced by activated T_h1, NK and $CD8^+$ T cells, enhances antigen presentation by activating proteasome subunits and regulators in addition to up-regulating the generation of either the MHC or TAP gene. IFN-γ alters proteasome activity by incorporation of three IFN-γ-inducible catalytic subunits, LMP2, LMP7 and MECL-1, to replace the constitutive catalytic subunits (Y/δ, X/MB1 and Z, respectively) in the 20S core particle during proteasome biogenesis (25, 41, 49). These IFN-γ-induced immunoproteasomes are speculated to be more favorable than constitutive proteasomes for antigen presentation because the subunits induced by IFN-γ stimulate cleavage after hydrophobic, basic and branched chain residues instead of acidic ones (50–54). There have been several reports on the importance of immunoproteasomes for the production of various MHC class I epitopes, although certain antigenic peptides are known to be generated by standard (or constitutive) proteasomes (26, 53).

It is reported that MECL-1 requires LMP2 for efficient incorporation into preproteasomes and LMP7 is required for efficient maturation of preproteasomes containing LMP2 and MECL-1 (54). On this basis, we employed LMP7-deficient mice to confirm the contribution of immunoproteasomes to protective immunity. In our study, anti-tumor immunity was profoundly attenuated in LMP7-deficient mice although not completely (Fig. 5). Thus, LMP7 appears to play an important role in the presentation of the MUT1 epitope on MHC class I molecules, probably synergistically with other immunoproteasome subunits such as LMP2 and/or MECL-1. Notably, we also found that a large proportion of ubiquitin-fused MUT1 underwent UFD after the serial attachment of ubiquitin (Fig. 4), despite the fact that MUT1 is a single 8-mer epitope for $CD8^+$ T cells.

Polyubiquitinated substrates are deubiquitinated at the entrances before passing through proteasomes. A constitutive 19S proteasome regulator (PA700) is known to be responsible for detachment of polyubiquitin at the entrance of the proteasome. This regulator may play an essential role in opening the gate, which is thought to increase the rate of peptide output (55), and prevent excessive degradation of epitopes by quick retrieval of properly degraded peptides from catalytic β-rings. As in the case with immunoproteasomes, IFN-γ plays a crucial role in the expression of two proteasome regulators PA28α and β, which form the heptameric proteasome activator complex PA28 (56). This heteromultimer has the potential to bind to the α rings of the 20S core particle, thereby enhancing proteolytic activity, although the mechanism of PA28-mediated enhancement of intrinsic core proteasome activity has not been fully elucidated (57). *In vitro* studies have shown that purified PA28α/β can enhance coordinated dual cleavage by the 20S proteasome, leading to augmented liberation of epitopes (58). Furthermore, expression of PA28α in mouse fibroblasts is known to increase the sensitivity to lysis by virus-specific CTLs (59). We found previously that processing of an epitope derived from the tumor antigen TRP-2 of murine B16 melanoma is entirely dependent on PA28α/β *in vitro* (33) and *in vivo* (34, 60). In this study, $PA28\alpha^{-/-}/\beta^{-/-}$ mice also failed to acquire anti-tumor immunity after immunization with pUB-MUT1 (Fig. 6).

Since the sequence of the oligonucleotides used to generate the fusion UB-MUT1 does not contain the stop codon, the construct used in this study is a little longer than the minimal sequence of eight amino acids. Accordingly, even the 8-mer CTL epitope may need to be manipulated by UPS, including PA28α/β, prior to presentation to MHC class I molecules and activating the corresponding $CD8^+$ T cells.

Another fascinating possibility regarding the role of UPS in the present system is that proteasomes have functions other than proteolytic activity. Epitopes passing through proteasomes readily find their way to TAP and are consequently transported to the endoplasmic reticulum, where they bind to MHC class I molecules. The precise roles of UPS in our system are still under investigation. It should be noted that the mutant mice used in this study, either $LMP7^{-/-}$ or $PA28\alpha^{-/-}/\beta^{-/-}$, showed no alteration in the ratio of $CD4^+$ and $CD8^+$ T cells to whole spleen or lymph node cells (data not shown).

This is believed to be the first report suggesting that DNA vaccination with a gene encoding a single $CD8^+$ T-cell epitope

in tumor antigens potently induces anti-tumor immunity when the gene has been fused with the ubiquitin gene, depending on the UPS.

Acknowledgements

We thank M. Sano for technical support. This work was supported by grants-in-aid from the Ministry of Education, Science, Sport, and Culture of Japan (15019075, 15025255, 15390136 and 15659265).

Abbreviations

APC	antigen-presenting cell
Con 37	connexin 37
3LL	Lewis lung carcinoma
TAA	tumor-associated antigen
TRP-2	tyrosinase-related protein 2
UFD	ubiquitin-fusion degradation pathway
UPS	ubiquitin–proteasome system

References

1 Mandelboim, O., Berke, G., Fridkin, M., Feldman, M., Eisenstein, M. and Eisenbach, L. 1994. CTL induction by a tumor associated antigen octapeptide derived from a murine lung carcinoma. *Nature* 369:67.

2 Boon, T., Gerottini, C. J., Van Der Eynde, B., Van Der Brugenn, P. and Van Pel, A. 1994. Tumor antigens recognized by T lymphocytes. *Annu. Rev. Immunol.* 12:337.

3 Boon, T. 1995. Tumor antigens and perspectives for cancer immunotherapy. *Immunologist* 3:262.

4 Cox, A. L., Skipper, J., Chen, Y. *et al.* 1994. Identification of a peptide recognized by five melanoma-specific human cytotoxic T cell lines. *Science* 264:716.

5 Rabinovich, N. R., McInnes, P., Klein, D. L. and Hall, B. F. 1994. Vaccine technologies: view to the future. *Science* 265:1401.

6 Mocellin, S., Mandruzzato, S., Bronte, V., Lise, M. and Nitti, D. 2004. Part I: vaccines for solid tumours. *Lancet Oncol.* 5:681.

7 Engelhard, V. H., Bullock, T. N., Colella, T. A., Sheasley, S. L. and Mullins, D. W. 2002. Antigens derived from melanocyte differentiation proteins: self-tolerance, autoimmunity, and use for cancer immunotherapy. *Immunol. Rev.* 188:136.

8 Ward, S., Casey, D., Labarthe, M. C. *et al.* 2002. Immunotherapeutic potential of whole tumour cells. *Cancer Immunol. Immunother.* 51:351.

9 Jaffee, E. M., Hruban, R. H., Biedrzychi, B. *et al.* 2001. Novel allogeneic granulocyte-macrophage colony-stimulating factor-secreting tumor vaccine for pancreatic cancer: a phase I trial of safety and immune activation. *J. Clin. Oncol.* 19:145.

10 Dranoff, G. 2002. GM-CSF-based cancer vaccines. *Immunol. Rev.* 188:147.

11 Song, K., Chang, Y. and Prud'homme, G. J. 2000. Regulation of T-helper-1 versus T-helper-2 activity and enhancement of tumor immunity by combined DNA-based vaccination and nonviral cytokine gene transfer. *Gene Ther.* 7:481.

12 Song, K., Chang, Y. and Prud'homme, G. J. 2000. IL-12 plasmid-enhanced DNA vaccination against carcinoembryonic antigen (CEA) studied in immune-gene knockout mice. *Gene Ther.* 7:1527.

13 Chakrabarti, R., Chang, Y., Song, K. and Pru'dhomme, G. J. 2004. Plasmids encoding membrane-bound IL-4 or IL-12 strongly costimulate DNA vaccination against carcinoembryonic antigen (CEA). *Vaccine* 22:1199.

14 Amici, A., Smorlesi, A., Noce, G. *et al.* 2000. DNA vaccination with full-length or truncated neu induces protective immunity against the development of spontaneous mammary tumors in HER-2/neu transgenic mice. *Gene Ther.* 7:703.

15 Di Carlo, E., Rovero, S., Boggio, K. *et al.* 2001. Inhibition of mammary carcinogenesis by systemic interleukin 12 or p185neu DNA vaccination in Her-2/neu transgenic BALB/c mice. *Clin. Cancer Res.* 7:830s.

16 Rovero, S., Boggio, K., Carlo, E. D. *et al.* 2001. Insertion of the DNA for the 163–171 peptide of IL1beta enables a DNA vaccine encoding p185 (neu) to inhibit mammary carcinogenesis in Her-2/neu transgenic BALB/c mice. *Gene Ther.* 8:447.

17 Piechocki, M. P., Ho, Y. S., Pilon, S. and Wei, W. Z. 2003. Human ErbB-2 (Her-2) transgenic mice: a model system for testing Her-2 based vaccines. *J. Immunol.* 171:5787.

18 Pilon, S. A., Piechocki, M. P. and Wei, W. Z. 2001. Vaccination with cytoplasmic ErbB-2 DNA protects mice from mammary tumor growth without anti-ErbB-2 antibody. *J. Immunol.* 167:3201.

19 Pasquini, S., Peralta, S., Missiaglia, E., Carta, L. and Lemoine, N. R. 2002. Prime-boost vaccines encoding an intracellular idiotype/GM-CSF fusion protein induce protective cell-mediated immunity in murine pre-B cell leukemia. *Gene Ther.* 9:503.

20 Timmerman, J. M., Singh, G., Hermanson, G. *et al.* 2002. Immunogenicity of a plasmid DNA vaccine encoding chimeric idiotype in patients with B-cell lymphoma. *Cancer Res.* 62:5845.

21 Hawkins, W. G., Gold, J. S., Dyall, R. *et al.* 2000. Immunization with DNA coding for gp100 results in CD4 T-cell independent antitumor immunity. *Surgery* 128:273.

22 Rakhmilevich, A. L., Imboden, M., Hao, Z. *et al.* 2001. Effective particle-mediated vaccination against mouse melanoma by coadministration of plasmid DNA encoding gp100 and granulocyte-macrophage colony-stimulating factor. *Clin. Cancer Res.* 7:952.

23 Kim, J. J., Yang, J. S., Dang, K., Manson, K. H. and Weiner, D. B. 2001. Engineering enhancement of immune responses to DNA-based vaccines in prostate cancer model in rhesus macaques through the use of cytokine gene adjuvants. *Clin. Cancer Res.* 7:882s.

24 Tanaka, K. and Kasahara, M. 1998. The MHC class I ligand-generating system: roles of immunoproteasomes and the interferon-gamma-inducible proteasome activator PA28. *Immunol. Rev.* 163:161.

25 Rock, K. L., York, I. A., Saric, T. and Goldberg, A. L. 2002. Protein degradation and the generation of MHC class I-presented peptides. *Adv. Immunol.* 80:1.

26 Kloetzel, P. M. 2001. Antigen processing by the proteasome. *Nat. Rev. Mol. Cell Biol.* 2:179.

27 Johnson, E. S., Ma, P. C., Ota, I. M. and Varshavsky, A. 1995. A proteolytic pathway that recognizes ubiquitin as a degradation signal. *J. Biol. Chem.* 270:17442.

28 Glickman, M. H. and Ciechanover, A. 2002. The ubiquitin-proteasome proteolytic pathway: destruction for the sake of construction. *Physiol. Rev.* 82:373.

29 Butt, T. R., Khan, M. I., Marsh, J., Ecker, D. J. and Crooke, S. T. 1988. Ubiquitin-metallothionein fusion protein expression in yeast. A genetic approach for analysis of ubiquitin function. *J. Biol. Chem.* 263:16364.

30 Johnson, E. S., Bartel, B., Seufert, W. and Varshavsky, A. 1992. Ubiquitin as a degradation signal. *EMBO J.* 11:497.

31 Murata, S., Udono, H., Tanahashi, N. *et al.* 2001. Immunoproteasome assembly and antigen presentation in mice lacking both PA28alpha and PA28beta. *EMBO J.* 20:5898.

32 Zhang, M., Obata, C., Hisaeda, H. *et al.* 2005. A novel DNA vaccine based on the ubiquitin-proteasome pathway targeting 'self'-antigen expressed in melanoma/melanocyte. *Gene Ther.* 12:1049.

33 Xiang, R., Lode, H. N., Chao, T. H. *et al.* 2000. An autologous oral DNA vaccine protects against murine melanoma. *Proc. Natl Acad. Sci. USA* 97:5492.

34 Wilson, C. C., McKinney, D., Anders, M. *et al.* 2003. Development of a DNA vaccine designed to induce cytotoxic T lymphocyte responses to multiple conserved epitopes in HIV-1. *J. Immunol.* 171:5611.

35 Bartholdy, C., Stryhn, A., Hansen, N. J., Buus, S. and Thomsen, A. R. 2003. Incomplete effector/memory differentiation of antigen-primed CD8+ T cells in gene gun DNA-vaccinated mice. *Eur. J. Immunol.* 33:1941.

36 Bartholdy, C., Olszewska, W., Stryhn, A., Thomsen, A. R. and Openshaw, P. J. 2004. Gene-gun DNA vaccination aggravates respiratory syncytial virus-induced pneumonitis. *J. Gen. Virol.* 85(Pt 10):3017.

37 Rasmussen, A. B., Zocca, M. B., Bonefeld, C. M. *et al.* 2004. Proteasomal targeting and minigene repetition improve cell-surface presentation of a transfected, modified melanoma tumour antigen. *Scand. J. Immunol.* 59:220.
38 Mandelboim, O., Bar-Haim, E., Vadai, E., Fridkin, M. and Eisenbach, L. 1997. Identification of shared tumor-associated antigen peptides between two spontaneous lung carcinomas. *J. Immunol.* 159:6030.
39 Fehling, H. J., Swat, W., Laplace, C. *et al.* 1994. MHC class I expression in mice lacking the proteasome subunit LMP-7. *Science* 265:1234.
40 Nishitani, M. A., Sakai, T., Ishii, K. *et al.* 2002. A convenient cancer vaccine therapy with *in vivo* transfer of interleukin 12 expression plasmid using gene gun technology after priming with irradiated carcinoma cells. *Cancer Gene Ther.* 9:156.
41 Sakai, T., Hisaeda, H., Nakano, Y. *et al.* 2000. Gene gun-mediated delivery of an interleukin-12 expression plasmid protects against infections with the intracellular protozoan parasites *Leishmania major* and *Trypanosoma cruzi* in mice. *Immunology* 99:615.
42 Sakai, T., Hisaeda, H., Nakano, Y. *et al.* 2003. Gene gun-based co-immunization of merozoite surface protein-1 cDNA with IL-12 expression plasmid confers protection against lethal *Plasmodium yoelii* in A/J mice. *Vaccine* 21:1432.
43 Matzinger, P. 1991. The JAM test. A simple assay for DNA fragmentation and cell death. *J. Immunol. Methods* 145:185.
44 Inaba, K., Young, J. W. and Steinman, R. M. 1987. Direct activation of CD8+ cytotoxic T lymphocytes by dendritic cells. *J. Exp. Med.* 166:182.
45 Steitz, J., Bruck, J., Gambotto, A., Knop, J. and Tuting, T. 2002. Genetic immunization with a melanocytic self-antigen linked to foreign helper sequences breaks tolerance and induces autoimmunity and tumor immunity. *Gene Ther.* 9:208.
46 Leitner, W. W., Hwang, L. N., deVeer, M. J. *et al.* 2003. Alphavirus-based DNA vaccine breaks immunological tolerance by activating innate antiviral pathways. *Nat. Med.* 9:33.
47 Koegl, M., Hoppe, T., Schlenker, S., Ulrich, H. D., Mayer, T. U. and Jentsch, S. 1999. A novel ubiquitination factor, E4, is involved in multiubiquitin chain assembly. *Cell* 96:635.
48 Richly, H., Rape, M., Braun, S., Rumpf, S., Hoege, C. and Jentsch, S. 2005. A series of ubiquitin binding factors connects CDC48/p97 to substrate multiubiquitylation and proteasomal targeting. *Cell* 120:73.
49 Kloetzel, P. M. and Ossendorp, F. 2004. Proteasome and peptidase function in MHC-class-I-mediated antigen presentation. *Curr. Opin. Immunol.* 16:76.
50 Driscoll, J., Brown, M. G., Finley, D. and Monaco, J. J. 1993. MHC-linked LMP gene products specifically alter peptidase activities of the proteasome. *Nature* 365:262.
51 Gaczynska, M., Rock, K. L. and Goldberg, A. L. 1993. Γ-interferon and expression of MHC genes regulate peptide hydrolysis by proteasomes. *Nature* 365:264.
52 Aki, M., Shimbara, N., Takashina, M. *et al.* 1994. Interferon-γ induces different subunit organizations and functional diversity of proteasomes. *J. Biochem.* 115:257.
53 Sijts, A., Zaiss, D. and Kloetzel, P. M. 2001. The role of the ubiquitin-proteasome pathway in MHC class I antigen processing: implications for vaccine design. *Curr. Mol. Med.* 1:665.
54 Griffin, T. A., Nandi, D., Cruz, M. *et al.* 1998. Immunoproteasome assembly: cooperative incorporation of interferon gamma (IFN-gamma)-inducible subunits. *J. Exp. Med.* 187:97.
55 Groettrup, M., Soza, A., Eggers, M. *et al.* 1996. A role for the proteasome regulator PA28alpha in antigen presentation. *Nature* 381:166.
56 Rechsteiner, M., Realini, C. and Ustrell, V. 2000. The proteasome activator 11 S REG (PA28) and class I antigen presentation. *Biochem. J.* 345(Pt 1):1.
57 Coux, O., Tanaka, K. and Goldberg, A. L. 1996. Structure and functions of the 20S and 26S proteasomes. *Annu. Rev. Biochem.* 65:801.
58 Dick, T. P., Ruppert, T., Groettrup, M. *et al.* 1996. Coordinated dual cleavages induced by the proteasome regulator PA28 lead to dominant MHC ligands. *Cell* 86:253.
59 Zhang, M., Ishii, K., Hisaeda, H. *et al.* 2004. Ubiquitin-fusion degradation pathway plays an indispensable role in naked DNA vaccination with a chimeric gene encoding a syngeneic cytotoxic T lymphocyte epitope of melanocyte and green fluorescent protein. *Immunology* 112:567.
60 Koehler, A., Cascio, P., Legget, D. S., Woo, K. M., Goldberg, A. L. and Finley, D. 2001. The axial channel of the proteasome core particle is gated by the Rpt2 ATPase and controls both substrate entry and product release. *Mol. Cell* 7:1143.

J. Antibiot. 59(12): 785–790, 2006

ORIGINAL ARTICLE

THE JOURNAL OF ANTIBIOTICS

Verticipyrone, a New NADH-fumarate Reductase Inhibitor, Produced by *Verticillium* sp. FKI-1083

Hideaki Ui, Kazuro Shiomi, Hideaki Suzuki, Hiroko Hatano, Hiromi Morimoto, Yuichi Yamaguchi, Rokuro Masuma, Toshiaki Sunazuka, Hiroyuki Shimamura, Kimitoshi Sakamoto, Kiyoshi Kita, Hideto Miyoshi, Hiroshi Tomoda, Satoshi Ōmura

Received: October 5, 2006 / Accepted: November 16, 2006

Abstract A new NADH-fumarate reductase inhibitor, verticipyrone, was isolated from the cultured broth of a fungus, *Verticillium* sp. FKI-1083. The structure was established as (*E*)-2-methoxy-3,5-dimethyl-6-(3-methyl-2-undecenyl)-4*H*-pyran-4-one. Verticipyrone exhibited an IC_{50} value of 0.88 nM against NADH-fumarate reductase of *Ascaris suum*. Verticipyrone inhibited both *Ascaris* and bovine heart complex I, and its synthetic analogue, 8,9-dihydro-8-hydroxyverticipyrone, showed good selectivity against *Ascaris* complex I.

Keywords verticipyrone, electron transport enzyme inhibitor, NADH-fumarate reductase

Introduction

Several electron transport inhibitors are in common practical use. A complex II inhibitor, siccanin, produced by *Helminthosporium siccans*, is used clinically for dermatophytosis, and analogues of a complex III inhibitor, strobilurin A, produced by *Strobilurus tenacellus*, are used for phytopathogenic fungi. In the course of screening for anthelmintic antibiotics, we have been interested in the differences in energy metabolisms between the host and helminths [1]. The NADH-fumarate reductase (NFRD) system, which is found in many anaerobic organisms, is part of a special respiratory system in parasitic helminths [2]. The system is composed of complex I (NADH-rhodoquinone oxidoreductase) and complex II (rhodoquinol-fumarate oxidoreductase). Electrons from NADH are accepted by rhodoquinone through complex I, and then transferred to fumarate through complex II. Though this anaerobic electron transport system is inefficient, it can provide ATP in the absence of oxygen. During our screening for inhibitors of NFRD using *Ascaris suum* (roundworm) mitochondria, we obtained nafuredin, atpenins, and paecilaminol from cultured broth of fungi. Nafuredin is a selective inhibitor of helminth complex I which showed anthelmintic activity *in vivo* [3, 4]. Atpenins are the most potent complex II inhibitors, useful as tools for biochemical studies, though the inhibition is non-selective between helminths and mammals [5]. Paecilaminol is the first amino alcohol that has NFRD inhibitory activity [6].

Further screening for NFRD inhibitors led to the

K. Shiomi (Corresponding author), **S. Ōmura** (Corresponding author), **H. Ui, R. Masuma, T. Sunazuka:** Kitasato Institute for Life Sciences and Graduate School of Infectious Control Sciences, Kitasato University, Minato-ku, Tokyo 108-8641, Japan, E-mail: shiomi@lisci.kitasato-u.ac.jp and omura-s@kitasato.or.jp
H. Shimamura: Graduate School of Infectious Control Sciences, Kitasato University, Minato-ku, Tokyo 108-8641, Japan
H. Morimoto, H. Tomoda: School of Pharmaceutical Sciences, Kitasato University, Minato-ku, Tokyo 108-8641, Japan
K. Shiomi, H. Suzuki, H. Hatano, Y. Yamaguchi, T. Sunazuka, S. Ōmura: The Kitasato Institute, Minato-ku, Tokyo 108-8642, Japan
K. Sakamoto, K. Kita: Department of Biomedical Chemistry, Graduate School of Medicine, The University of Tokyo, Hongo, Bunkyo-ku, Tokyo 113-0033, Japan
H. Miyoshi: Division of Applied Life Sciences, Graduate School of Agriculture, Kyoto University, Kitashirakawa Oiwake-cho, Sakyo-ku, Kyoto 606-8502, Japan

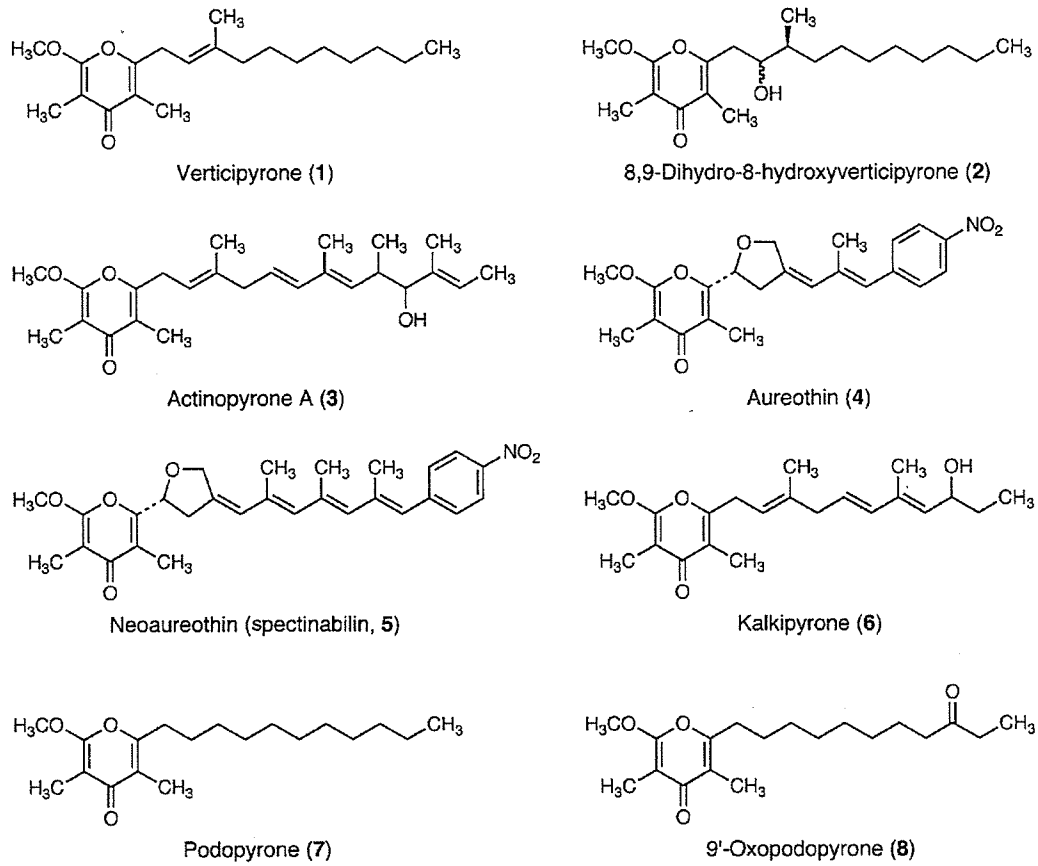

Fig. 1 Structures of verticipyrone (**1**) and related γ-pyrones (**2**~**8**).

isolation of a new compound, verticipyrone (**1**, Fig. 1), produced by a cultured broth of *Verticillium* sp. FKI-1083 [7]. The structure of **1** contains 2-methoxy-3,5-dimethyl-γ-pyrone similar to that of actinopyrone A (**3**) [8, 9], aureothin (**4**) [10~12], neoaureothin (spectinabilin, **5**) [13~15], kalkipyrone (**6**) [16], and podopyrones (**7**, **8**) [17~19]. In this report, we describe the taxonomy of the producing strain and the fermentation, isolation, structure elucidation, and biological properties of **1**. Selective inhibition of *A. suum* complex I by a synthetic analogue, 8,9-dihydro-8-hydroxyverticipyrone, (**2**) is also shown.

Results and Discussion

Taxonomy and Producing Strain FKI-1083

Strain FKI-1083 (Fig. 2) was isolated from a soil sample collected on Yakushima Island, Kagoshima Prefecture, Japan. The strain was taxonomically determined as genus *Verticillium* sp. The strain has been deposited at International Patent Organism Depository, the National Institute of Advanced Industrial Science and Technology, Tsukuba, Japan, as FERM BP-7804.

Fermentation and Isolation of Verticipyrone

A stock culture of the strain FKI-1083 was inoculated into a 500-ml Erlenmeyer flask containing 100 ml of a seed medium. After incubation on a rotary shaker (200 rpm) at 27°C for 3 days, one milliliter of the seed culture was transferred into each of twenty 500-ml Erlenmeyer flasks containing 100 ml of a production medium. The fermentation was carried out on a rotary shaker (200 rpm) at 27°C for 7 days.

Mycelia were collected from the cultured broth (2 liters) by centrifugation. The pellet was treated with methanol, and the extracted methanol solution was evaporated *in vacuo* to remove methanol. The aqueous extract was partitioned with ethyl acetate, and the organic layer was concentrated to dryness *in vacuo* to afford a crude material (1.21 g). This was applied on a silica gel column (Merck Art. 7734) and washed with *n*-hexane - ethyl acetate (3 : 1). Active fractions eluted with *n*-hexane - ethyl acetate (1 : 1)

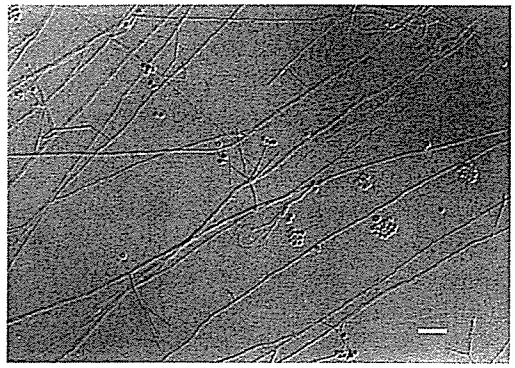

Fig. 2 Photomicrograph of phialide and conidia of *Verticillium* sp. FKI-1083. Bar represents 20 μm.

were concentrated to yield a crude material (81.0 mg), which was then chromatographed over another silica gel column. The column was packed with *n*-hexane - ethyl acetate (2 : 1) and active fractions were eluted with *n*-hexane - ethyl acetate (2 : 1). The elution afforded a colorless oil of **1** (61.1 mg)

Structure Elucidation of Verticipyrone

Physico-chemical properties of **1** are summarized in Table 1. The molecular formula of **1** was established as $C_{20}H_{32}O_3$ by HR-FAB-MS.

Chemical shifts of **1** in the ^1H and ^{13}C NMR are shown in Table 2. Analysis of the ^1H NMR, ^{13}C NMR, DEPT, and HMQC spectra revealed the presence of six quaternary, one methine, eight methylene, and five methyl carbons. A γ-pyrone ring was established on the basis of HMBC data (Fig. 3). A methoxy group 2-OCH_3 (δ_H 4.00) showed correlation to a polarized olefinic carbon C-2 (δ 164.5), and the C-2 correlated with a vinyl methyl 3-CH_3 (δ_H 1.80). The 3-CH_3 had further correlations to another polarized olefinic carbon C-3 (δ 100.1) and a conjugated carbonyl C-4 (δ 183.1). The C-4 carbonyl showed correlation to a vinyl methyl 5-CH_3 (δ_H 1.94), and the 5-CH_3 correlated with the second set of polarized olefinic carbons, C-5 (δ 118.7) and C-6 (δ 160.1). Therefore, a 2-methoxy-3,5-dimethyl-γ-pyrone ring was suggested, and UV absorption at 250 nm and IR absorption at 1670 cm^{-1} (C=O) are consistent with the previous data for related compounds [9, 11, 14~19]

The structure of 3-methyl-2-undecenyl side chain (C-7~C-17) attached to C-6 was deduced by ^1H-^1H COSY and HMBC as shown in Fig. 3. The geometrical isomerism of the olefin was elucidated as *E* by the chemical shift of 9-CH_3 (δ_C 16.3) [20]. Correlations between H_2-16 (δ 1.28) and H_3-17 (δ 0.88) in ^1H-^1H COSY and HMBC among 15, 16, and 17 positions suggested the terminal linear structure of the hydrocarbon chain. Though the remaining two methylenes could not be assigned because protons from H_2-12 to H_2-15 showed almost the same chemical shifts, they should be included into the hydrocarbon chain. Thus,

Table 1 Physico-chemical properties of **1**

Appearance	Colorless oil
Molecular formula	$C_{20}H_{32}O_3$
Molecular weight	320.47
HR-FAB-MS (*m/z*)	
found	343.2247 $(M+Na)^+$
calcd	343.2249 for $C_{20}H_{32}O_3Na$
UV λ_{max}^{MeOH} nm (ε)	204 (20,500), 215 (sh, 13,720), 250 (10,460)
IR ν_{max} (KBr) cm^{-1}	2927, 2854, 1732, 1670, 1605, 1464, 1408, 1379, 1325, 1250, 1165
Solubility	
Soluble	$CHCl_3$, EtOAc, MeOH
Insoluble	H_2O, *n*-hexane
Color reaction	
Positive	H_2SO_4, I_2

Table 2 ^1H and ^{13}C data of **1**[a]

Position	δ_C (mult)	δ_H (int, *J* (Hz))
2	164.5 s	
3	100.1 s	
4	183.1 s	
5	118.7 s	
6	160.1 s	
7	30.8 t	3.40 d (2H; 7.2)
8	118.2 d	5.26 t (1H, 7.2)
9	140.7 s	
10	40.5 t	2.06 t (2H, 7.6)
11	28.8 t	1.43 m (2H)
12	30.5 t	1.26 m (8H)
13	30.4 t	
14	30.2 t	
15	33.0 t	
16	23.7 t	1.28 m (2H)
17	14.4 q	0.88 t (3H 7.2)
2-OCH_3	56.4 q	4.00 s (3H)
3-CH_3	7.0 q	1.80 s (3H)
5-CH_3	10.0 q	1.94 s (3H)
9-CH_3	16.3 q	1.76 s (3H)

[a] NMR spectra were recorded on a Varian Inova 600 spectrometer. Chemical shifts are shown in δ value (ppm) relative to CD_3OD at 3.30 ppm for ^1H NMR and at 49.8 ppm for ^{13}C NMR.

the structure of **1** was elucidated as (*E*)-2-methoxy-3,5-dimethyl-6-(3-methyl-2-undecenyl)-4*H*-pyran-4-one (Fig. 1).

Biological Activities of Verticipyrone

We evaluated inhibitory activities of **1** against each complex using submitochondrial particles of *A. suum* and bovine heart (Table 3). Compound **1** inhibited NFRD from *A. suum* with an IC_{50} value of 0.88 nM and the inhibition was specific to NADH-rhodoquinone oxidoreductase (complex I). It also inhibited NADH-ubiquinone oxidoreductase (complex I) from bovine heart to the same extent as *A. suum* enzymes. However, the IC_{50} values differed greatly between NFRD and NADH-rhodoquinone oxidoreductase of *A. suum* and between NADH oxidase and NADH-ubiquinone oxidoreductase of bovine heart. This may be due to the difference of quinone concentration. Endogenous quinones were used for NFRD and NADH oxidase assays, while rhodoquinone and ubiquinone were added exogenously for NADH-quinone oxidoreductase assays. Therefore, the latter assays contained higher concentration of quinones, and competitive (or partially competitive) inhibitors may have reduced their inhibition.

We have accomplished the total synthesis of **1** and prepared some analogues of **1** [21]. Among them, 8,9-dihydro-8-hydroxyverticipyrone (**2**) showed potent inhibition against *Ascaris* complex I (IC_{50}=2.0 nM).

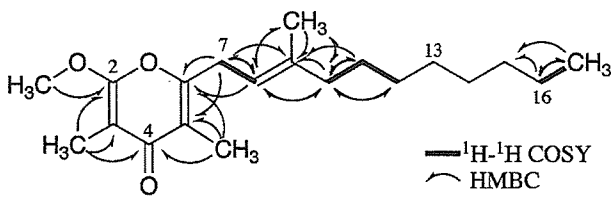

Fig. 3 Selected ^1H-^1H COSY and HMBC correlations of **1**.

The inhibition of **2** against bovine heart complex I was 100 times less potent, and **2** exhibited good selectivity to *Ascaris* complex I. The similarity of the IC_{50} values between NFRD and NADH-rhodoquinone oxidoreductase of *A. suum* suggested that **2** may not competitive to rhodoquinone at *Ascaris* complex I inhibition. Further studies are required to clarify the inhibitory mechanisms of these compounds.

Compound **1** is produced by a fungus and has 6-substituted-2-methoxy-3,5-dimethyl-4*H*-pyran-4-one. Such compounds are found from not only fungi but also cyanobacteria, actinomycetes, and plants. Among them, aureothin (**4**) was reported to have a complex I inhibitory activity [12]. We found that neoaureothin (**5**) inhibited NFRD at IC_{50} value of 15 nM. A γ-pyrone with a side chain seems to be essential to inhibit complex I, but interestingly, **4** is not competitive to the structurally-related substrate, quinone [12].

Nematocidal and insecticidal activities of **1** were studied by a microplate assay using the free-living nematode *Caenorhabditis elegans* and brine shrimp *Artemia salina*. Minimum growth inhibitory concentrations of **1** against *C. elegans* and *A. salina* were 20 μg/ml and 2.0 μg/ml, respectively. Kalkipyrone (**6**) was reported to show similar toxicity against brine shrimp (LD_{50}=1 μg/ml) [16]. As shown in Table 4, **1** exhibited moderate antimicrobial activity against Gram-positive bacteria. Actinopyrone A (**3**) exhibited weak antimicrobial activities against some Gram-positive bacteria and dermatophytes, in addition to coronary vasodilating activities in anaesthetized dogs [9].

Experimental

General

NMR spectra were recorded on a Varian Inova 600

Table 3 Inhibition of NFRD and NADH oxidase by **1** and **2**

Origin	Enzyme	Complex	IC_{50} [nM]	
			1	**2**
A. suum	NADH-fumarate reductase	I+II	0.88	1.5
	NADH-rhodoquinone oxidoreductase	I	49	2.0
	Rhodoquinol-fumarate oxidoreductase	II	>100,000	>100,000
Bovine heart	NADH oxidase	I+III+IV	1.3	20
	NADH-ubiquinone oxidoreductase	I	46	200
	Succinate-ubiquinone oxidoreductase	II	>100,000	>100,000
	Ubiquinol-cytochrome *c* oxidoreductase	III	26,000	80,000

Table 4 Antimicrobial activity of **1**

Microorganisms	MIC (μg/ml)
Staphylococcus aureus ATCC6538P	6.25
Bacillus subtilis ATCC6633	6.25
Micrococcus luteus ATCC9341	6.25
Mycobacterium smegmatis ATCC607	12.5
Escherichia coli NIHJ	>100
Escherichia coli IFO12734	>100
Pseudomonas aeruginosa IFO3080	>100
Xanthomonas campestris pv. *oryzae* KB88	>100
Candida albicans KF1	>100
Saccharomyces cerevisiae KF26	>100
Aspergillus niger ATCC6275	100
Mucor racemosus IFO4581	100
Acholeplasma laidlawii PG8 KB174	>50
Bacteroides fragilis ATCC23745	>50

spectrometer ($^{2\text{-}3}J_{CH}$=8 Hz in HMBC). Chemical shifts are shown in δ values (ppm) relative to CD_3OD at 3.30 ppm for ^1H NMR and at 49.8 ppm for ^{13}C NMR. Mass spectrometry was conducted on a JEOL JMS-AX505 HA spectrometer. The UV and IR spectra were measured with Shimadzu UV-240 spectrophotometer and Horiba FT-210 Fourier transform infrared spectrometer, respectively.

Taxonomic Studies of the Producing Organism

Morphological observations of the verticipyrone-producing strain were carried out using an Olympus Vanox-S AH-2 microscope.

Media

The seed medium consisted of glucose 2.0%, Polypepton (Nihon Pharmaceutical Co.) 0.5%, yeast extract (Oriental Yeast Co.) 0.2%, KH_2PO_4 0.1%, $MgSO_4 \cdot 7H_2O$ 0.05%, and agar 0.1%, pH 5.7. The production medium consisted of potato dextrose broth (Difco) 2.4%, malt extract (Difco) 1.5%, $MgPO_4 \cdot 8H_2O$ 0.5%, and agar 0.1%, pH 6.0.

Biological Studies

Submitochondrial particles were prepared from adult *A. suum* and bovine heart and used for electron transport enzyme assays. The enzyme assays were performed as described previously [3]. The assay method for nematocidal and insecticidal activities was reported previously [22]. The antimicrobial activity was measured by agar dilution method.

Acknowledgements We are grateful to Dr. Achim Harder of Bayer HealthCare AG, Animal Health-Research & Development-Parasiticides for valuable discussions. We also thank Ms. Akiko Nakagawa and Ms. Chikako Sakabe of the School of Pharmaceutical Sciences, Kitasato University for measurements of mass spectra. This work was supported by a Grant-in-Aid for Scientific Research (14593006 to K.S. and 17790274 and 18GS0314 to K.K.) and a Grant-in-Aid for Encouragement of Young Scientists (12771373 to H.U.). This work was also supported in part by Grant of the 21st Century COE Program, Ministry of Education, Culture, Sports, Science, and Technology.

References

1. Komuniecki R, Tielens AGM. Carbohydrate and energy metabolism in parasitic helminths. *In* Molecular Medical Parasitology. *Ed.*, J. J. Marr, *et al.*, pp. 339–358, Academic Press, London (2003)
2. Kita K, Nihei C, Tomitsuka E. Parasite mitochondria as drug target: diversity and dynamic changes during the life cycle. Curr Med Chem 10: 2535–2548 (2003)
3. Ōmura S, Miyadera H, Ui H, Shiomi K, Yamaguchi Y, Masuma R, Nagamitsu T, Takano D, Sunazuka T, Harder A, Kölbl H, Namikoshi M, Miyoshi H, Sakamoto K, Kita K. An anthelmintic compound, nafuredin, shows selective inhibition of complex I in helminth mitochondria. Proc Natl Acad Sci USA 98: 60–62 (2001)
4. Ui H, Shiomi K, Yamaguchi Y, Masuma R, Nagamitsu T, Takano D, Sunazuka T, Namikoshi M, Ōmura S. Nafuredin, a novel inhibitor of NADH-fumarate reductase, produced by *Aspergillus niger* FT-0554. J Antibiot 54: 234–238 (2001)
5. Miyadera H, Shiomi K, Ui H, Yamaguchi Y, Masuma R, Tomoda H, Miyoshi H, Osanai A, Kita K, Ōmura S. Atpenins, potent and specific inhibitors of mitochondrial complex II (succinate-ubiquinone oxidoreductase). Proc Natl Acad Sci USA 100: 473–477 (2003)
6. Ui H, Shiomi K, Suzuki H, Hatano H, Morimoto H, Yamaguchi Y, Masuma R, Sakamoto K, Kita K, Miyoshi H, Tomoda H, Tanaka H, Ōmura S. Paecilaminol, a new NADH-fumarate reductase inhibitor, produced by *Paecilomyces* sp. FKI-0550. J Antibiot 59: 591–596 (2006)
7. Ōmura S, Shiomi K, Masuma R. Novel substance FKI-1083 and process for producing the same. PCT Int Appl, WO/2003/050104, June 19 (2003)
8. Yano K, Yokoi K, Sato J, Oono J, Kouda T, Ogawa Y, Nakashima T. Actinopyrones A, B and C, new physiologically active substances. I. Producing organism, fermentation, isolation and biological properties. J Antibiot 39: 32–37 (1986)
9. Yano K, Yokoi K, Sato J, Oono J, Kouda T, Ogawa Y, Nakashima T. Actinopyrones A, B and C, new physiologically active substances. II. Physico-chemical properties and chemical structures. J Antibiot 39: 38–43 (1986)
10. Maeda K. Chemical studies on antibiotic substances, IV. A crystalline toxic substance of *Streptomyces thioluteus*

producing aureothricin. J Antibiot A 6: 137–138 (1953)
11. Hirata Y, Nakata H, Yamada K, Okuhara K, Naito T. The structure of aureothin, a nitro compound obtained from *Streptomyces thioluteus*. Tetrahedron 14: 252–274 (1961)
12. Friedrich T, Van Heek P, Leif H, Ohnishi T, Forche E, Kunze B, Jansen R, Trowitzsch-Kienast W, Höfle G, Reichenbach H, Weiss H. Two binding sites of inhibitors in NADH: ubiquinone oxidoreductase (complex I). Relationship of one site with the ubiquinone-binding site of bacterial glucose: ubiquinone oxidoreductase. Eur J Biochem 219: 691–698 (1994)
13. Cassinelli G, Grein A, Orezzi P, Pennella P, Sanfilippo A. New antibiotics produced by *Streptoverticillium orinoci*, n. sp. Arch Mikrobiol 55: 358–368 (1967)
14. Cardani C, Ghiringhelli D, Selva A, Arcamone F, Camerino B, Cassinelli G. The structure of neoaureothin. Chim Ind 52: 793–794 (1970)
15. Kakinuma K, Hanson CA, Rinehart KL Jr. Spectinabilin, a new nitro-containing metabolite isolated from *Streptomyces spectinabilis*. Tetrahedron 32: 217–222 (1976)
16. Graber MA, Gerwick WH. Kalkipyrone, a toxic γ-pyrone from an assemblage of the marine cyanobacteria *Lyngbya majuscula* and *Tolypothrix* sp. J Nat Prod 61: 677–680 (1998)
17. Zdero C, Bohlmann F, King RM, Robinson H. Pyrone derivatives from *Podolepis hieracioides* and sesquiterpene acids from *Cassinia longifolia*. Phytochemistry 26: 187–190 (1987)
18. Jaensch M, Jakupovic J, King RM, Robinson H. Pyrones and other constituents from *Podolepis* species. Phytochemistry 28: 3497–3501 (1989)
19. Kanazawa T, Ohkawa Y, Kuda T, Minobe Y, Tani T, Nishizawa M. γ-Pyrones from *Gonystylus keitheii*, as new inhibitors of parathyroid hormone (PTH)-induced Ca release from neonatal mouse calvaria. Chem Pharm Bull 45: 1046–1051 (1997)
20. Barlow L, Pattenden G. Synthesis of poly-*Z*-isomers of 2,6,11,15-tetramethylhexadeca-2,6,8,10,14-pentaene, a C_{20} analogue of phytoene. Re-examination of the stereochemistry of a new isomer of phytoene from *Rhodospirillum rubrum*. J Chem Soc Perkin I 1976: 1029–1034 (1976)
21. Shimamura H, Sunazuka T, Izuhara T, Hirose T, Shiomi K, Ōmura S. Total synthesis of verticipyrone, and biological evaluation of its synthetic analogues. Org Lett (in press)
22. Enomoto Y, Shiomi K, Matsumoto A, Takahashi Y, Iwai Y, Harder A, Kölbl H, Woodruff HB, Ōmura S. Isolation of a new antibiotic oligomycin G produced by *Streptomyces* sp. WK-6150. J Antibiot 54: 308–313 (2001)

J. Antibiot. 59(9): 591–596, 2006

ORIGINAL ARTICLE

THE JOURNAL OF ANTIBIOTICS

Paecilaminol, a New NADH-Fumarate Reductase Inhibitor, Produced by *Paecilomyces* sp. FKI-0550

Hideaki Ui, Kazuro Shiomi, Hideaki Suzuki, Hiroko Hatano, Hiromi Morimoto, Yuichi Yamaguchi, Rokuro Masuma, Kimitoshi Sakamoto, Kiyoshi Kita, Hideto Miyoshi, Hiroshi Tomoda, Haruo Tanaka, Satoshi Ōmura

Received: July 12, 2006 / Accepted: August 24, 2006

Abstract A new NADH-fumarate reductase inhibitor, paecilaminol, was isolated from the cultured broth of a fungus *Paecilomyces* sp. FKI-0550. It is an amino alcohol compound, the structure being established as 2-amino-14,16-dimethyl-3-octadecanol. Paecilaminol exhibited an IC_{50} value of 5.1 μM against *Ascaris suum* NADH-fumarate reductase.

Keywords paecilaminol, electron transport enzyme inhibitor, NADH-fumarate reductase

Introduction

Microorganisms produce many useful antiparasitic antibiotics [1]. In the course of screening for anthelmintic antibiotics, we have been interested in the differences in energy metabolisms between the host and helminths [2]. The NADH-fumarate reductase (NFRD) system, which is found in many anaerobic organisms, is part of a special respiratory system in parasitic helminths [3]. The system is composed of complex I (NADH-rhodoquinone oxidoreductase) and complex II (rhodoquinol-fumarate oxidoreductase). Electrons from NADH are accepted by rhodoquinone through complex I, and then transferred to fumarate through complex II. This anaerobic electron transport system can provide ATP in the absence of oxygen. During our screening for inhibitors of NFRD using *Ascaris suum* (roundworm) mitochondria, we obtained both nafuredin and atpenins. Nafuredin is a selective inhibitor of helminth complex I which showed anthelmintic activity *in vivo* [4, 5]. Atpenins are complex II inhibitors, and the inhibition is non-selective between helminths and mammals [6]. They are the most potent complex II inhibitors and are expected to be useful tools for biochemical studies.

Further screening for NFRD inhibitors led to the isolation of a new compound, paecilaminol (**1**, Fig. 1), which was produced by a cultured broth of *Paecilomyces* sp. FKI-0550 [7]. In this report, we describe the taxonomy of the producing strain and the fermentation, isolation, structure elucidation, and biological properties of **1**.

K. Shiomi (Corresponding author), **S. Ōmura** (Corresponding author), **H. Ui, R. Masuma:** Kitasato Institute for Life Sciences and Graduate School of Infection Control Sciences, Kitasato University, 5-9-1 Shirokane, Minato-ku, Tokyo 108-8641, Japan, E-mail: shiomi@lisci.kitasato-u.ac.jp and omura-s@kitasato.or.jp
H. Morimoto, H. Tomoda: School of Pharmaceutical Sciences, Kitasato University, 5-9-1 Shirokane, Minato-ku, Tokyo 108-8641, Japan
K. Shiomi, H. Suzuki, H. Hatano, Y. Yamaguchi, H. Tanaka, S. Ōmura: The Kitasato Institute, 5-9-1 Shirokane, Minato-ku, Tokyo 108-8642, Japan
K. Sakamoto, K. Kita: Department of Biomedical Chemistry, Graduate School of Medicine, The University of Tokyo, Hongo, Bunkyo-ku, Tokyo 113-0033, Japan
H. Miyoshi: Division of Applied Life Sciences, Graduate School of Agriculture, Kyoto University, Kitashirakawa Oiwake-cho, Sakyo-ku, Kyoto 606-8502, Japan

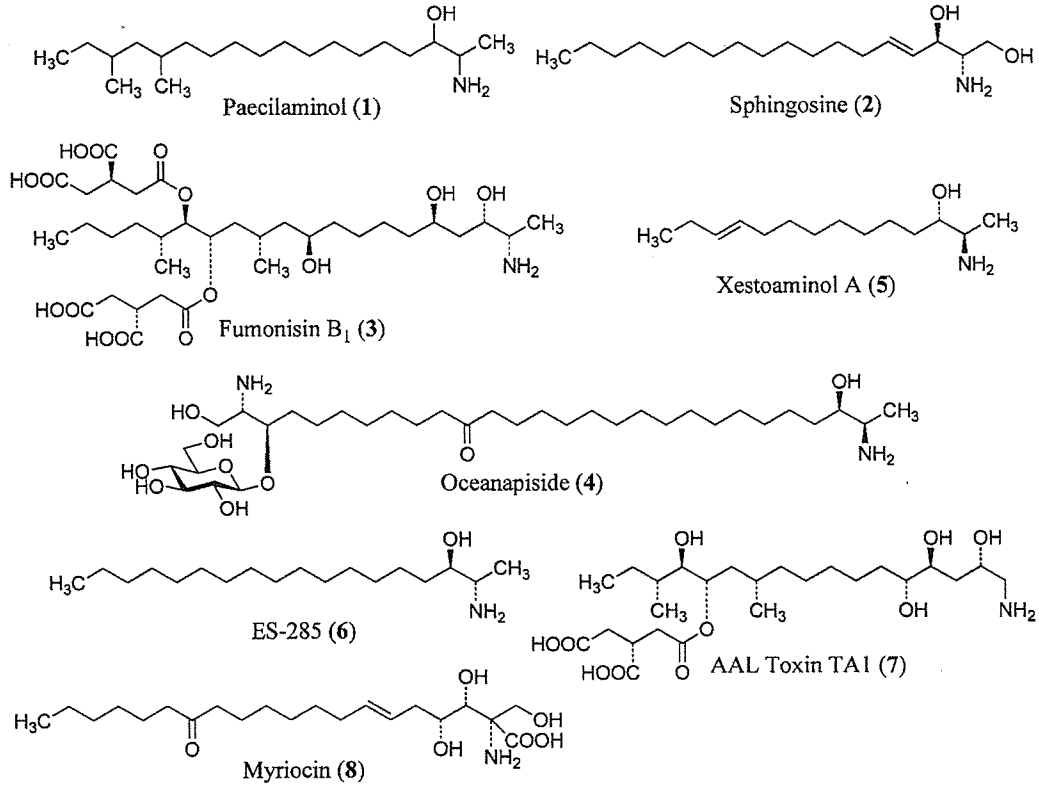

Fig. 1 Structures of paecilaminol (**1**) and related amino alcohols (**2**~**8**).

Results and Discussion

Taxonomy of Producing Strain FKI-0550

Strain FKI-0550 was originally isolated from a soil sample collected on Miyakojima Island, Okinawa Prefecture, Japan. The strain was taxonomically determined as genus *Paecilomyces* sp. The strain has been deposited at the International Patent Organism Depositary, National Institute of Advanced Industrial Science and Technology, Tsukuba, Japan, as FERM BP-7785.

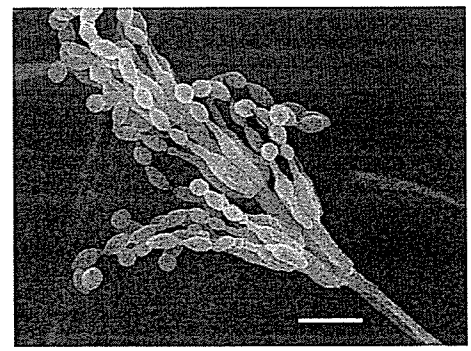

Fig. 2 Scanning electron micrograph of strain FKI-0550. Bar represents 5 μm.

Fermentation and Isolation of Paecilaminol

A stock culture of the strain FKI-0550 was inoculated into two 500-ml Erlenmeyer flasks containing 100 ml of a seed medium and incubated on a rotary shaker at 27°C for 3 days. One milliliter of the seed culture was transferred into each of one hundred 500-ml Erlenmeyer flasks containing 100 ml of a production medium. The fermentation was carried out on a rotary shaker at 27°C for 9 days.

Mycelia were collected from the cultured broth (10 liters) by centrifugation. They were treated with methanol, the extract removed and the methanol was evaporated. The aqueous extract was partitioned with ethyl acetate, and the organic layer was concentrated to dryness *in vacuo* to afford a crude material (461 mg). This was applied on a silica gel column (Merck Art. 7734) and washed with $CHCl_3$-methanol (10 : 1). Active fractions eluted with $CHCl_3$-methanol (1 : 1) were concentrated to yield a crude material (120 mg), which was then chromatographed over another silica gel column. The column was washed with

ethyl acetate and eluted with ethyl acetate - methanol - concd NH_4OH (80 : 9 : 1). The elution afforded a pale yellow oil of **1** (70.1 mg).

Structure Elucidation of Paecilaminol

Physico-chemical properties of **1** are summarized in Table 1. The molecular formula of **1** was established as $C_{20}H_{43}NO$ by HR-FAB-MS. The IR absorbances observed at 2958, 2924, 2852, 1464, and 1377 cm^{-1} suggested the presence of saturated methyl and methylene groups. The absorbance at 1574 cm^{-1} suggested an amino group, and the absorbances at 3300 and 1080 cm^{-1} suggested a hydroxyl and/or amino group. As the index of hydrogen deficiency of **1** was 0, **1** was suggested to be an alkyl amino alcohol. This was further supported by the analysis of IR absorbances.

Chemical shifts of **1** in the ^1H and ^{13}C NMR are shown in Table 2. Analysis of the ^1H NMR, ^{13}C NMR, DEPT, and HMQC spectra revealed the presence of four methine, twelve methylene, and four methyl carbons. ^1H-^1H-COSY of **1** indicated the presence of 3-amino-2-hydroxybutyl (C-1 to C-4) and 2,4-dimethylhexyl (C-13 to C-18) moieties (Fig. 3). Long-range couplings from 3-H (δ 3.16) and 4-H_2 (δ 1.33 and 1.46) to C-5 (δ 25.8) suggested the bond between C-4 and C-5, and the couplings from 13-H_2 (δ 1.01 and 1.26) and 14-H (δ 1.45) to C-12 (δ 26.9) suggested the bond between C-12 and C-13 in HMBC. Though the remaining six methylenes could not be assigned as their protons showed almost the same chemical shifts, they should be linked to the two moieties. Thus, the structure of **1** was elucidated as 2-amino-14,16-dimethyl-3-octadecanol (Fig. 1). After our patent publication [7], **1** was reported to be isolated from *Fusarium avenaceum* as a cytotoxic compound [8].

Table 1 Physico-chemical properties of **1**

Appearance		pale yellow oil
$[\alpha]_D^{25}$		+26.7° (*c* 0.24, MeOH)
Molecular formula		$C_{20}H_{43}NO$
Molecular weight		313.57
HR-FAB-MS (*m/z*)	found	314.3424 $(M+H)^+$
	calcd	314.3423 for $C_{20}H_{44}NO$
UV λ_{max}^{MeOH} nm (ε)		203 (8,250), 220 (sh, 4,400), 246 (2,040), 265 (sh, 1,570)
IR ν_{max} (KBr) cm^{-1}		3300, 2958, 2924, 2852, 1574, 1464, 1377, 1080
Solubility	soluble	$CHCl_3$, EtOAc, MeOH, CH_3CN
	insoluble	*n*-hexane
Color reaction	positive	ninhydrin, H_2SO_4

Table 2 ^1H and ^{13}C data (in $CDCl_3$) of **1**[a]

Position	δ_C (mult)	δ_H (int, *J* (Hz))
1	20.9 q	1.09 d (3H, 6.3)
2	51.1 d	2.72 dq (1H, 6.4, 6.3)
3	75.6 d	3.16 m (1H)
4	34.2 t	1.33 m (1H), 1.46 m (1H)
5	25.8 t	1.33 m (1H), 1.46 m (1H)
6	30.03[b] t	1.25 m (12H)
7~10	29.62 t	
	29.63 t	
	29.65 t	
	29.69 t	
11	29.8[b] t	
12	26.9 t	1.26 m (2H)
13	36.9 t	1.01 m (1H), 1.26 m (1H)
14	30.01 d	1.45 m (1H)
14-CH_3	20.3 q	0.82 d (3H, 6.6)
15	44.7 t	0.88 ddd (1H, 14.0, 7.0, 7.0), 1.20 m (1H)
16	31.6 d	1.40 m (1H)
16-CH_3	19.7 q	0.82 d (3H, 6.6)
17	29.2 t	1.05 m (1H), 1.33 m (1H)
18	11.2 q	0.84 dd (3H, 7.4, 7.4)

[a] NMR spectra were recorded on a Varian Inova 600 spectrometer. Chemical shifts are shown in δ values (ppm) relative to $CDCl_3$ at 7.26 ppm for ^1H NMR and at 77.0 ppm for ^{13}C NMR.
[b] The chemical shifts are interchangeable.

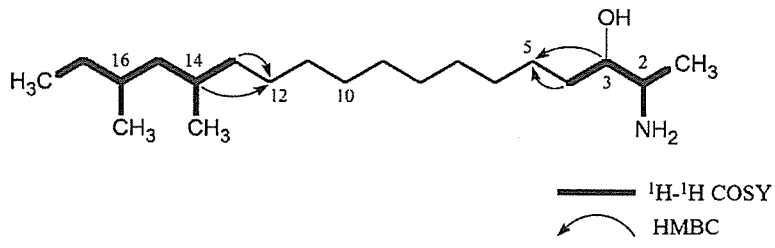

Fig. 3 Selected ^1H-^1H COSY and HMBC correlations of **1**.